A PICTURE is worth a thousand *words:*

Understanding the Visual Impact of the *Wilmington East* Offshore Wind Tract Area

January 2022

Dear Reader,

Rapid population growth, the desire to generate new economic opportunity, particularly in the eastern part of the state, and the natural endowment of the state's coastline point to offshore wind as an important component of North Carolina's future clean energy mix. Accordingly, offshore wind represents one pillar of the state's plans to achieve a 70% reduction in carbon emissions based on 2005 levels by 2030 and net zero carbon emissions by 2050.

Yet, as with any new technology, we understand that concerns remain regarding how offshore wind will be developed and deployed. One of these concerns relates to the potential visual impact of wind turbines off the North Carolina coast. Key questions include: Will wind turbines be visible from the beach? How will the turbines appear at different times of day and under varying weather conditions?

In this study, developed with the support of the British Consulate in Atlanta, we have relied on our deep expertise, backgrounds and cutting edge software in engineering, computer modelling, and data analysis, coupled with our several decades of experience modelling both offshore oil and gas fields and more recently offshore wind tracts in our native United Kingdom (see appendix UNA for our company profile), to create a sophisticated and realistic model of the visual impact that will result from current plans for offshore wind development at the Wilmington East Wind Energy Area.

Upon conducting this analysis, and as clearly illustrated in the images and data that follow, our professional assessment and conclusion is that the wind turbines at the Wilmington East site will be minimally visible from only those locations closest to the project site, and not at all visible from the vast majority of the proximal towns and beaches. Thus, the overall visual impact of the project from shore will be negligible.

Our report begins with a summary of top-line conclusions, followed by key assumptions underpinning our analysis. We then share seven photos that illustrate the visual impact of the proposed wind turbines from Bald Head Island (Viewing Point 1), Oak Island (Viewing Point 2), and Holden Beach (Viewing Point 3). These photos are accompanied with succinct descriptions of the conditions under which the modelling occurred. In the appendix, we have included additional technical specifications for those with an interest in digging in further to the specifics.

As the saying goes, "A picture is worth a thousand words." Thank you for taking the time to read our assessment and we hope that you find it of value in understanding the anticipated visual impact for the Wilmington East offshore wind tract.

Respectfully,

Mick Flynn

Partner
Unasys

CONCLUSIONS

- The wind turbines will appear close to the horizon and only form a very small part of the human field of view.
- While two different weather conditions were modelled, the photos with a hazier sky are most relevant since those weather conditions prevail on most days of the year, and are most common in summer.
- At distances of 17 nautical miles and greater, it is very difficult for the naked eye to delineate between the ocean, the horizon, and the visible blade tips, making the Wilmington East Wind Energy Area barely visible from shore.
- Bald Head Island extends from the North Carolina mainland more than 8 miles compared to the next closest beach. The vast majority of North Carolina beaches are too far from the project location to be able to view the wind turbines, and those that are within distance are more than 27 nautical miles away.
- Any substations for the development would be in the central space in the middle of the field. These units are not normally greater than 50 metres above sea level and therefore would be out of sight, due to the curvature of the earth.
- Technology will ensure that night-time aviation lights are off unless aircraft are in the vicinity. According to our calculations, the tower obstruction lights would only be visible on 5 wind turbines and that would only be from VP1 on Bald Head Island. Obstruction lights are of medium intensity and would be very difficult to see with the naked eye from shore. See VP3 Image 3.

Key Specifications and Assumptions

To enable us to create the visualisations, we first needed to establish the field layout, and to help us to optimize that layout, we needed to understand the weather patterns running through the field.

Ten-year weather and wind data was collected and the resulting turbine layout employs industry best practice of siting turbines in an aligned array with a longer streamwise turbine spacing, suitable for locations with fixed prevailing wind direction.

The Wilmington East Wind Energy Area

The Wilmington East Wind Energy Area (shown in red below), as defined by the US Department of Interior's Bureau of Ocean Energy Management (BOEM) as of January 2022, begins about 17 nautical miles from Bald Head Island at its closest point and extends approximately 18 nautical miles in the southeast direction to its furthest point from land. It will contain approximately 25 Outer Continental shelf blocks and covers 133,590 acres.

(Outer Continental Shelf (OCS) lease blocks serve as the legal definition for BOEM offshore boundary coordinates used to define small geographic areas within an Official Protraction Diagram (OPD) for leasing and administrative purposes.)

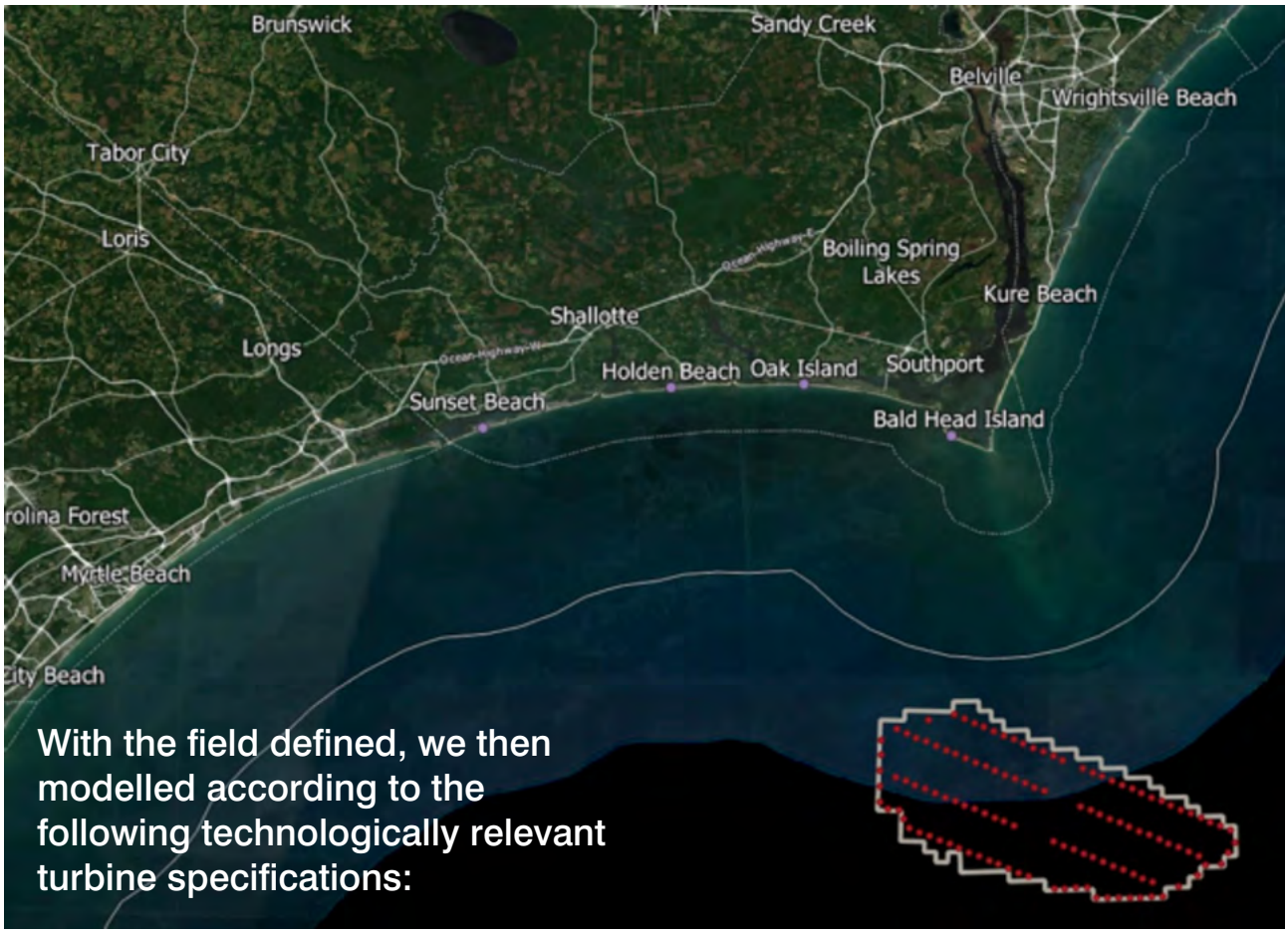

- Turbines simulated: GE Haliade -X 13MW
- Height of turbine at nacelle centre: 524 feet (150 metres)
- Number of wind turbines – 122
- Height at highest point (highest blade tip): 853 feet (260 metres)
- Rotor diameter: 722 feet (220 metres)
- Above-water support structure: Single pole that is 20 feet (6 metres) at the waterline, or as specified for turbine model
- Colour of wind turbines: Off-white (5% grey) Substations: None have been simulated, but space has been added for two units in the field. Those units would be of approximate height and dimensions: 114 feet by 82 feet by 50 feet (35 metres by 25 metres by 15 metres)
- Lighting: two aviation warning lights spec L864 fixtures duty and standby on top of the nacelle. Medium intensity flashing red. Three L810 marine traffic obstruction fixtures at 120-degree spacings around the perimeter of the tower, halfway between the sea and the nacelle. This number would increase to four should the diameter of the tower be more than 20 feet (6 metres)

VISUALIZATIONS

In 2012 BOEM conducted a comprehensive visual impact assessment for hypothetical wind farms off of North Carolina's shore. All data and information can be viewed at: https://*www.boem.gov/renewable-energy/state-activities/offshore-north-carolina-visualization-study.*

Because this study utilized standard distances from shore (10, 15, and 20 nautical miles) as well as much smaller turbines, which were the most technologically advanced at that time, it made sense to do a more specific analysis of the current Wilmington East Wind Energy Area, and its known distance from shore, with current turbine technology – larger, but fewer turbines. Therefore, this analysis utilizes the photos taken for that analysis and applies the updated parameters.

There are three viewing points for our visualizations, representing the three beaches closest to the wind energy area:

VP1 Bald Head Island
VP2 Oak Island
VP3 Holden Beach

VP1 *Bald Head Island* has two day time visuals showing hazy and polarized conditions at a viewing angle of 41 degrees.

VP2 ***Oak Island*** has two day time visuals showing hazy and polarized conditions at 37 degrees.

VP3 *Holden Beach* has two day time visuals showing hazy and polarized conditions at 37 degrees and one night time visual under a clear night condition at 37 degrees.

Weather conditions, including haze, have a significant effect on visibility. As was outlined in BOEM's 2012 visibility report, most days off the NC coast are hazy. One can only see as far as 20 nautical miles for 11% (40 days) of the year.

Compared to other seasons, summer days have the highest amount of haze/humidity, making it more difficult to see further distances. It is more common to experience clear days/nights in the winter when humidity and air pollutants are at their lowest levels.

To make the distinction between the more commonly experienced hazy conditions, and a perfectly clear condition, photographs with two different lenses were used – a polarized lens simulating a haze free sky, and a UV lens simulating a more common hazy/humid condition.

When printed at 1200 dpi or higher on a color printer and quality 11"x17" paper at actual size, the single-frame simulations will be in proper perspective and resolution when viewed at 23.5" from the eye.

If viewed on a monitor, use the highest screen resolution possible and view at a distance of approximately twice the image height.

Camera Specification

Nikon D7000 16.2 MP DSLRCamera / Nikkor AF-S DX 35mm fixed lens

- A +/-50mm lens on a 35mm camera is an industry standard for preparing single-frame photographic simulations
- The Nikkor 35mm fixed lens mounted on the Nikon D7000 produces an equivalent to a 52.5mm lens on a 35mm camera
- Nikkor DX 35mm lens captures a horizontal angle of 37.3° and vertical angle of 25.3°, or 2,238-by-1,518 arcminutes
- The Nikon D7000 highest resolution image is 4,928-by-3,264 pixels 16MP (This was upgraded to 70MP by Unasys utilizing artificial intelligence software)
- Each pixel subtends 0.45 arcminutes, which is less than the maximum of 0.5 arcminutes.

VP1 Bald Head Island

Date	April 14, 2012
Time of Day	3 p.m.
Viewpoint Elevation	16 feet
Camera Height	5 feet 6 inches
Sun Angle/Azimuth	247.9 degrees
Lighting Angle	Front lit
Sun Elevation	44.7 degrees
Observed Weather	Partly cloudy
Lat/long	(33.8579 -78.0026)
Original photos used	BHA_336, BHA_337 BHA_338, BHA_421 BHA_422, BHA_423

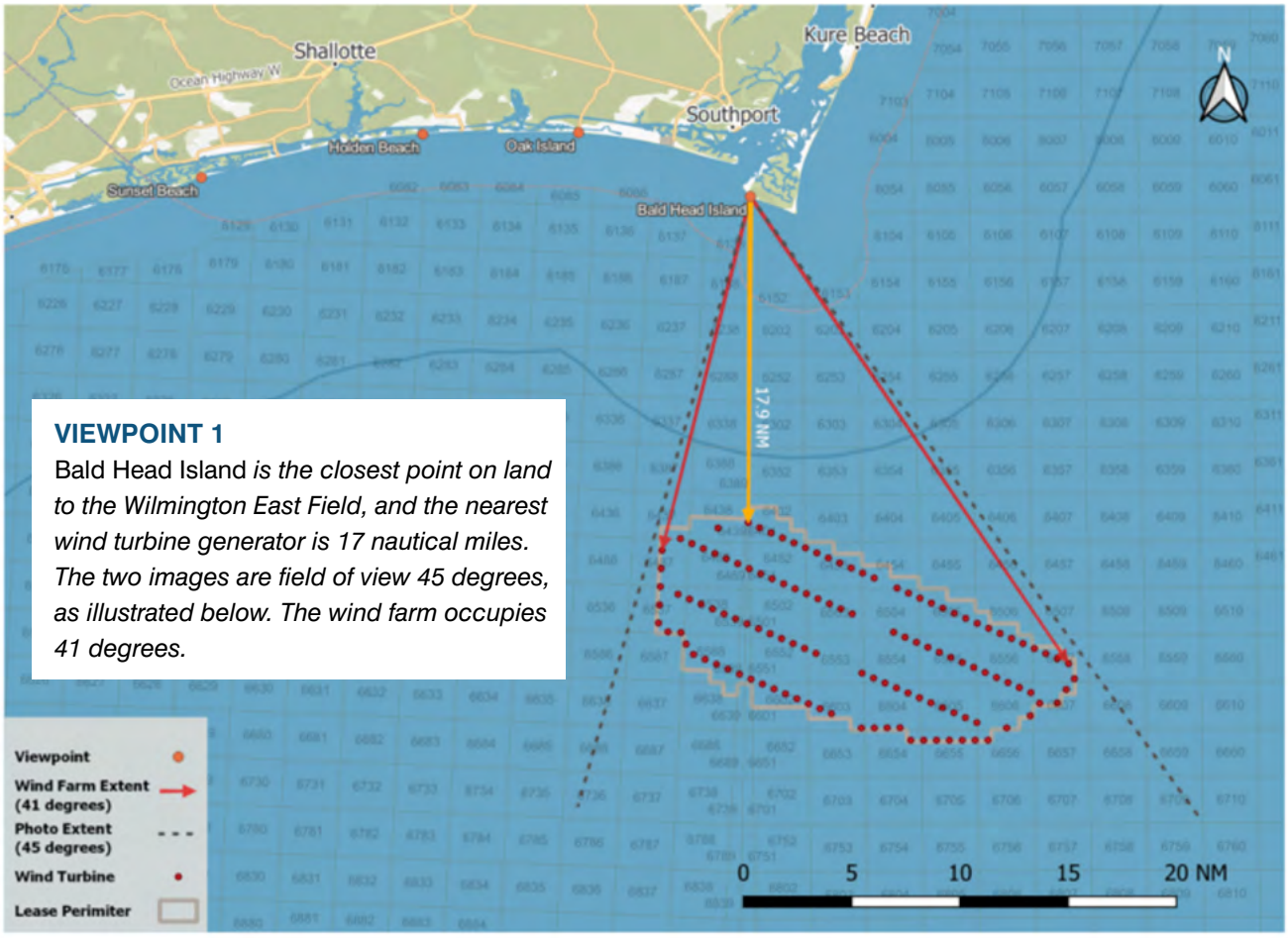

VIEWPOINT 1

Bald Head Island *is the closest point on land to the Wilmington East Field, and the nearest wind turbine generator is 17 nautical miles. The two images are field of view 45 degrees, as illustrated below. The wind farm occupies 41 degrees.*

VP1 Image 1 Bald Head Island Average Day

This first image is on a clear sunny day, with an ultraviolet filter giving a slightly hazy or real-life horizon.

This view is to be expected approximately 80% of the year based on annual historical weather patterns.

Haze is caused by tiny particles that scatter and absorb light before it reaches an observer's eye. As the number of particles increases, more light is absorbed and scattered, resulting in less clarity, diffused colour, and limited visual range.

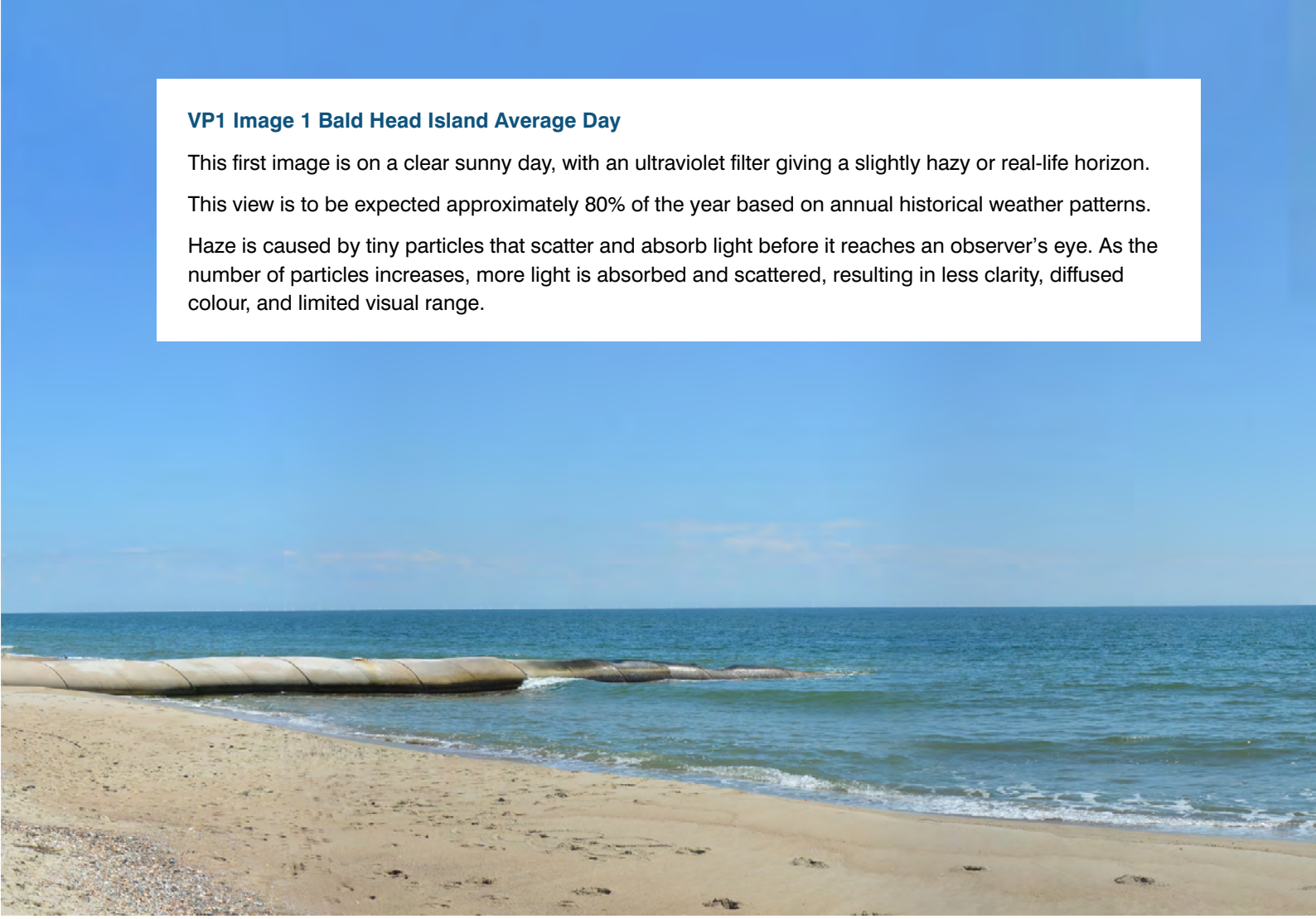

VP1 Image 2 Bald Head Island Clear Day

This image is on a clear sunny day, with a clear polarized horizon. This view is expected 20% of the year based on historical average weather patterns.

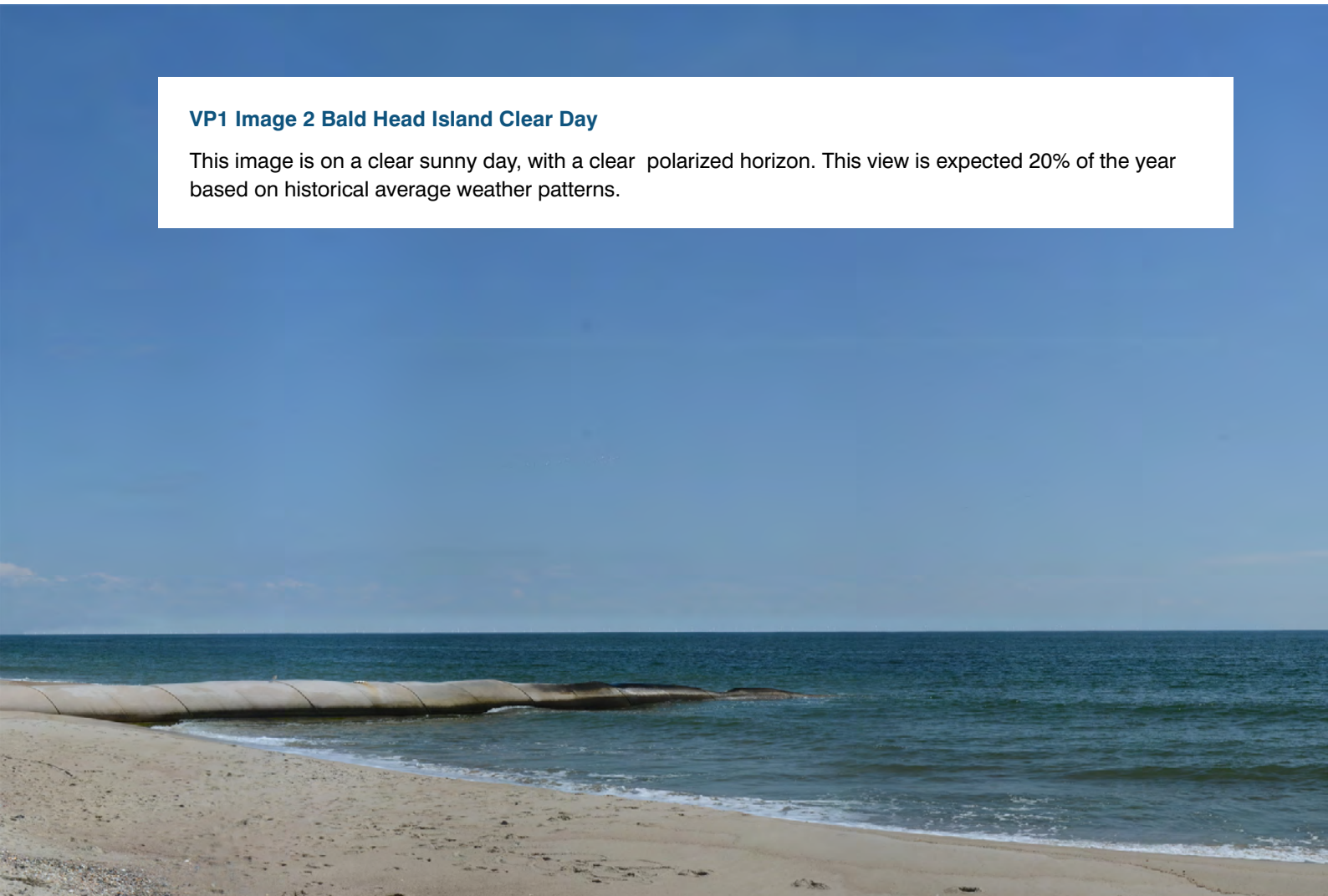

VP2 Oak Island

Date	April 14, 2012
Time of Day	6 p.m.
Viewpoint Elevation	9 feet
Camera Height	5 feet 6 inches
Sun Angle/Azimuth	276.5 degrees
Lighting Angle	Side lit
Sun Elevation	8.1 degrees
Observed Weather	Partly cloudy
Lat/Long	(33.91384 -78.1612)
Original images used	OIA_467,OIA_468 OIA_544, OIA_545

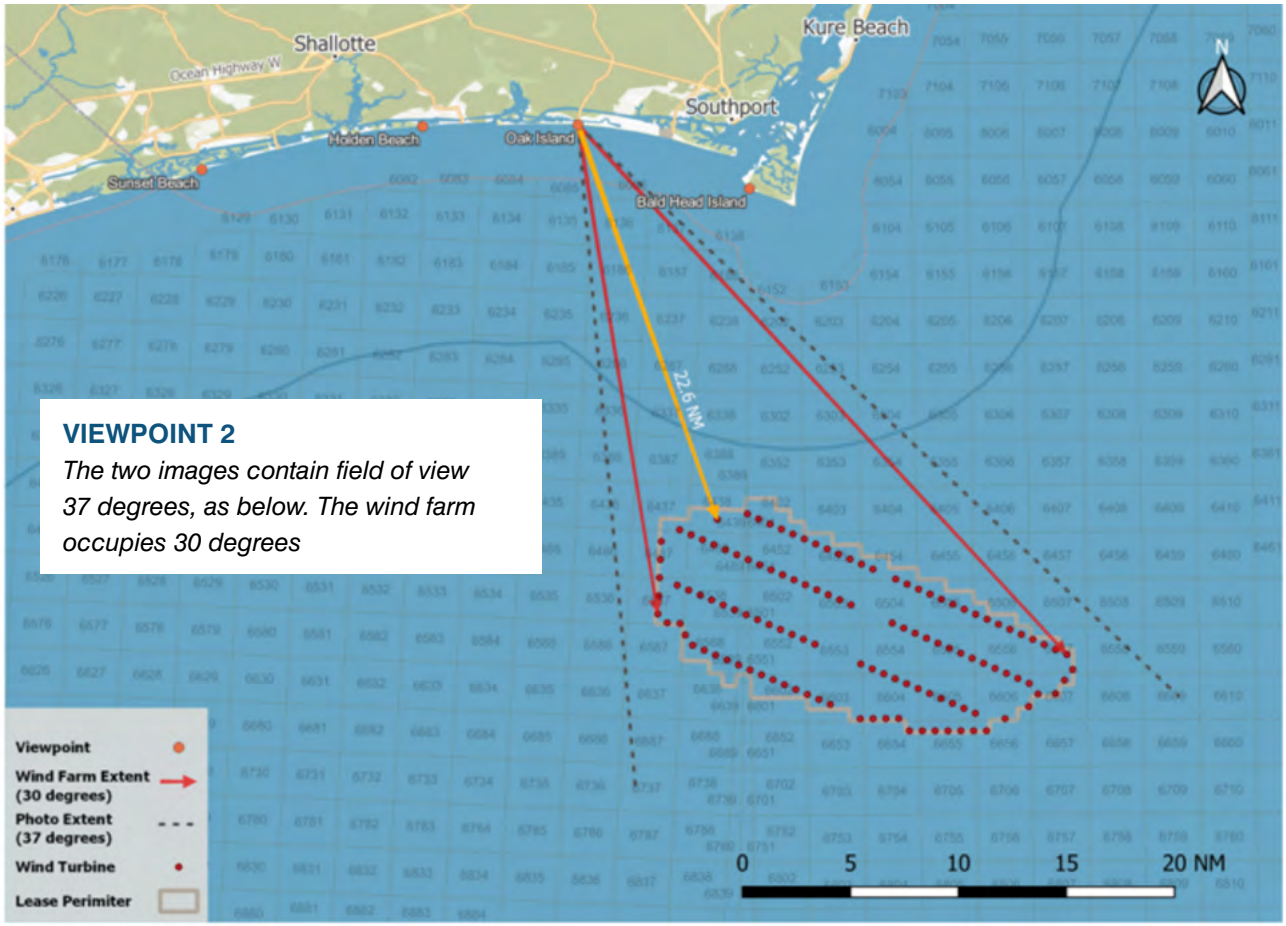

VP2 Image 1 Oak Island Average Day

This first image is on a clear sunny day, with an ultraviolet filter giving a slightly hazy or real-life horizon.

This view is to be expected approximately 80% of the year based on annual historical weather patterns.

Haze is caused by tiny particles that scatter and absorb light before it reaches an observer's eye. As the number of particles increases, more light is absorbed and scattered, resulting in less clarity, diffused colour, and limited visual range.

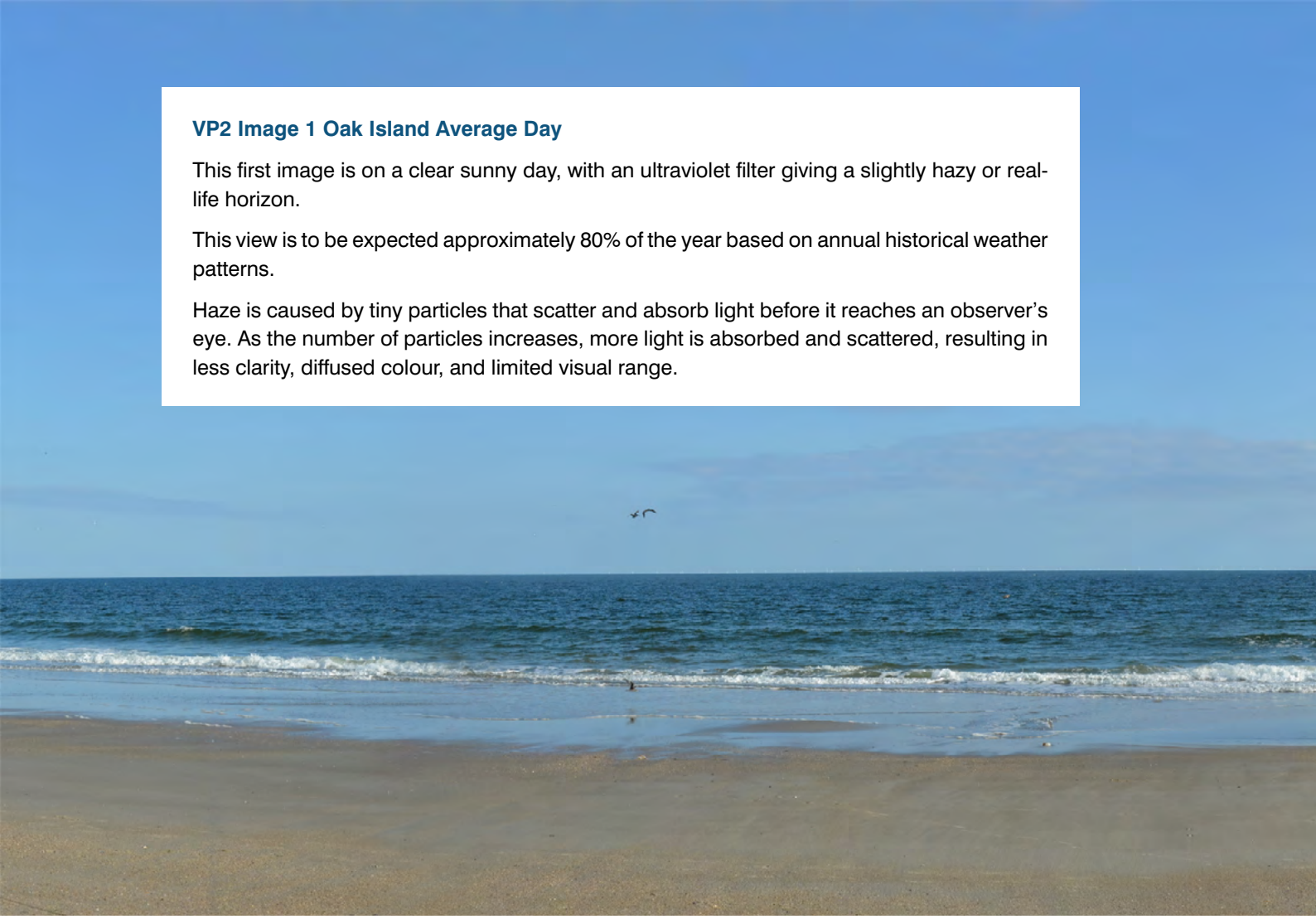

VP2 Image 2 Oak Island Clear Day

This image is on a clear sunny day, with a clear polarized horizon. This view is expected 20% of the year based on historical average weather patterns.

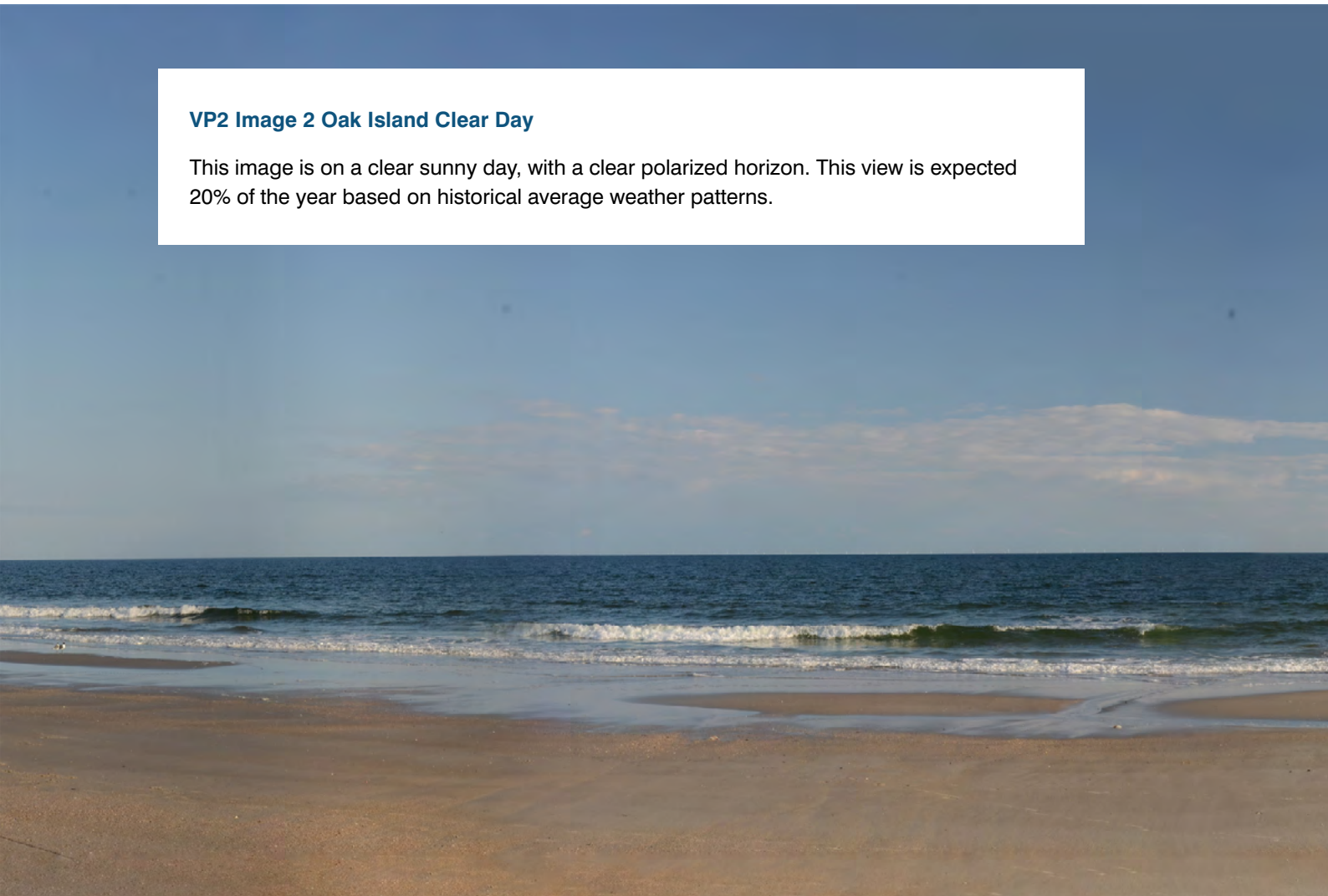

VP3 Holden Beach

Date	13 April 2012
Time of Day	6 p.m.
Viewpoint Elevation	6 feet
Camera Height	5 feet 6 inches
Sun Angle/Azimuth	276 degrees
Lighting Angle	Side lit
Sun Elevation	8.1 degrees
Observed Weather	Partly cloudy
Lat/Long	(33.9100 -78.3042)
Original images used	HBA_163, HBA164 HBA_164, HBA_204 HBA_205, HBA_594 HBA_595

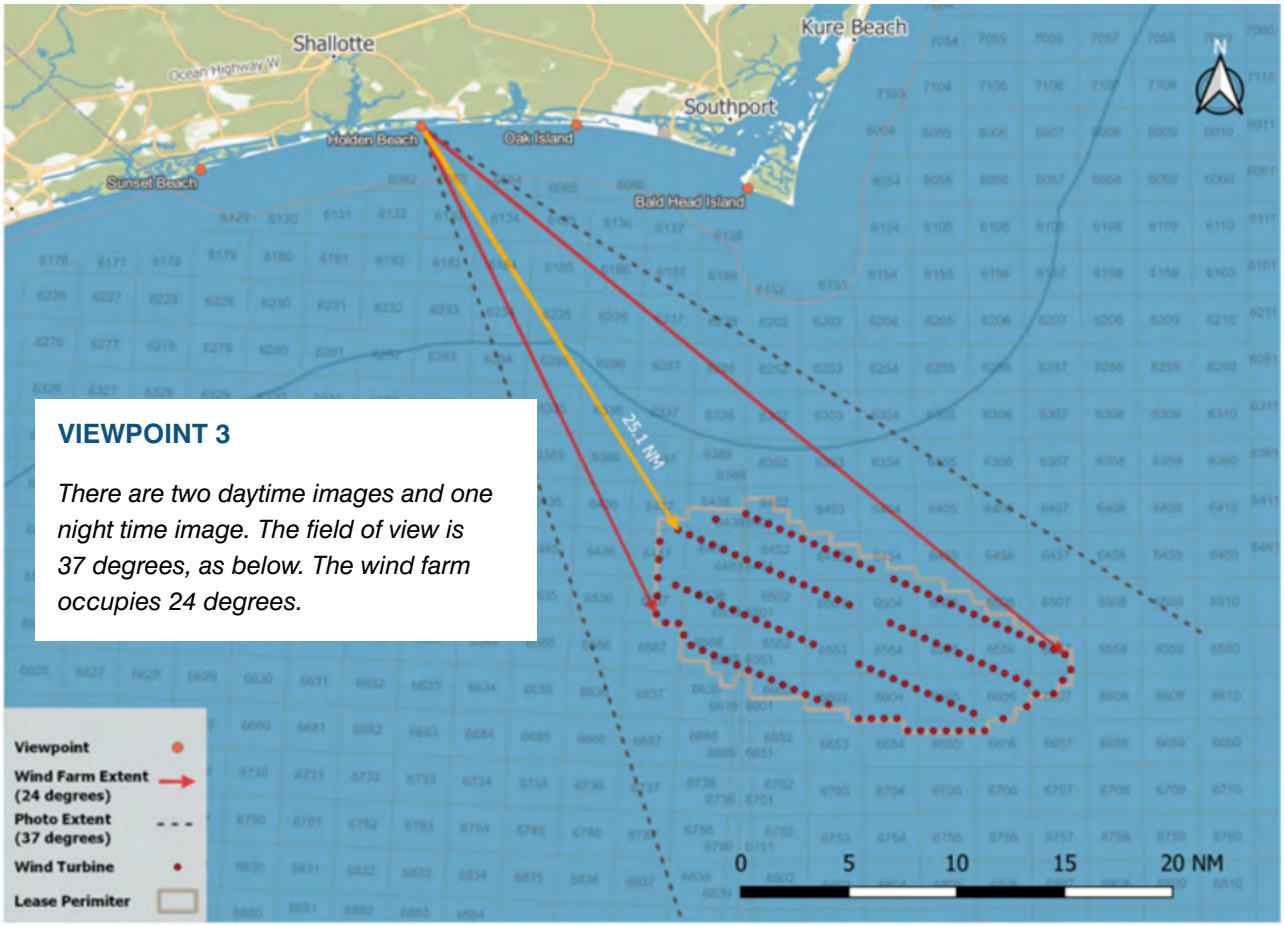

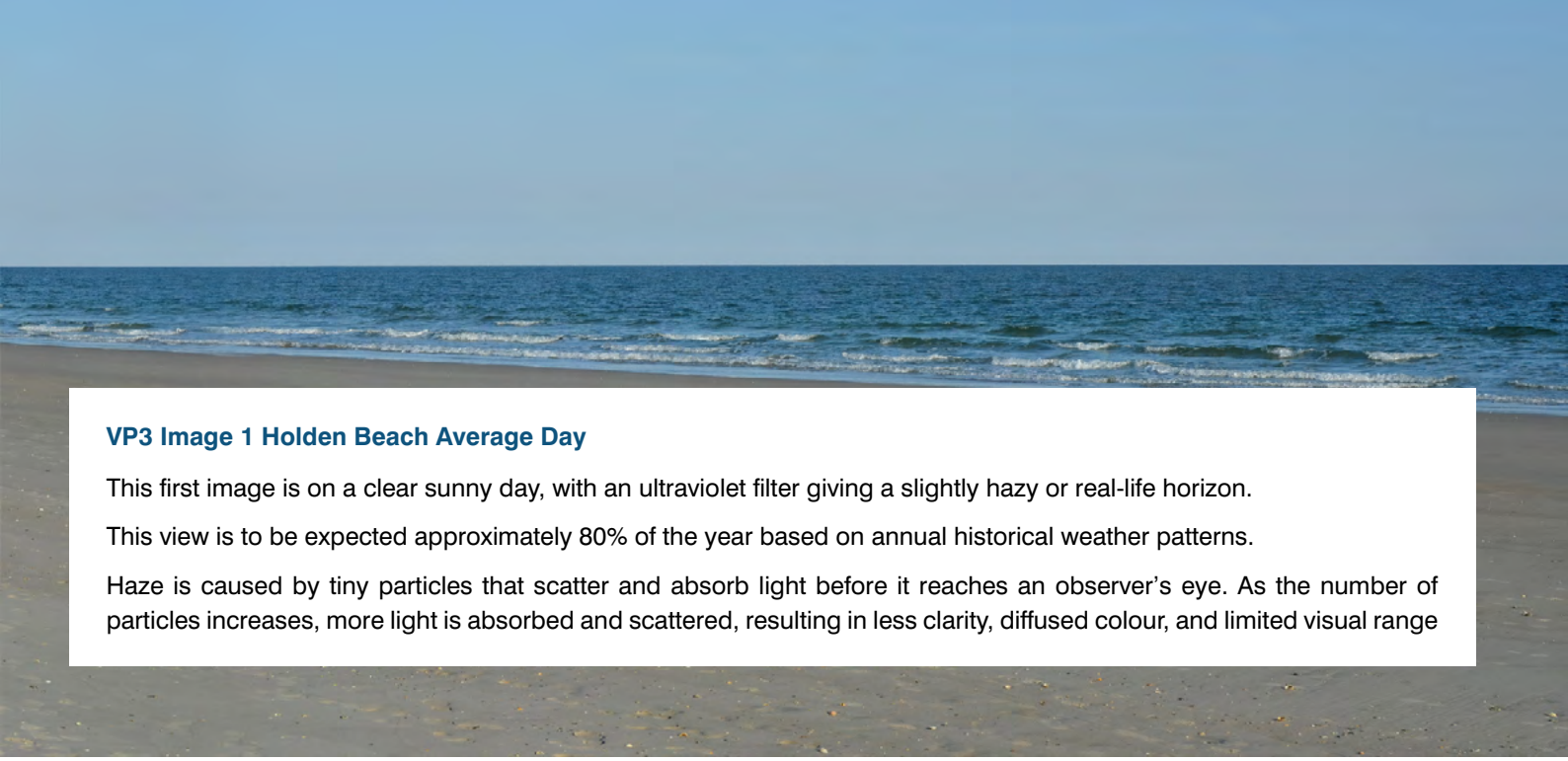

VP3 Image 1 Holden Beach Average Day

This first image is on a clear sunny day, with an ultraviolet filter giving a slightly hazy or real-life horizon.

This view is to be expected approximately 80% of the year based on annual historical weather patterns.

Haze is caused by tiny particles that scatter and absorb light before it reaches an observer's eye. As the number of particles increases, more light is absorbed and scattered, resulting in less clarity, diffused colour, and limited visual range

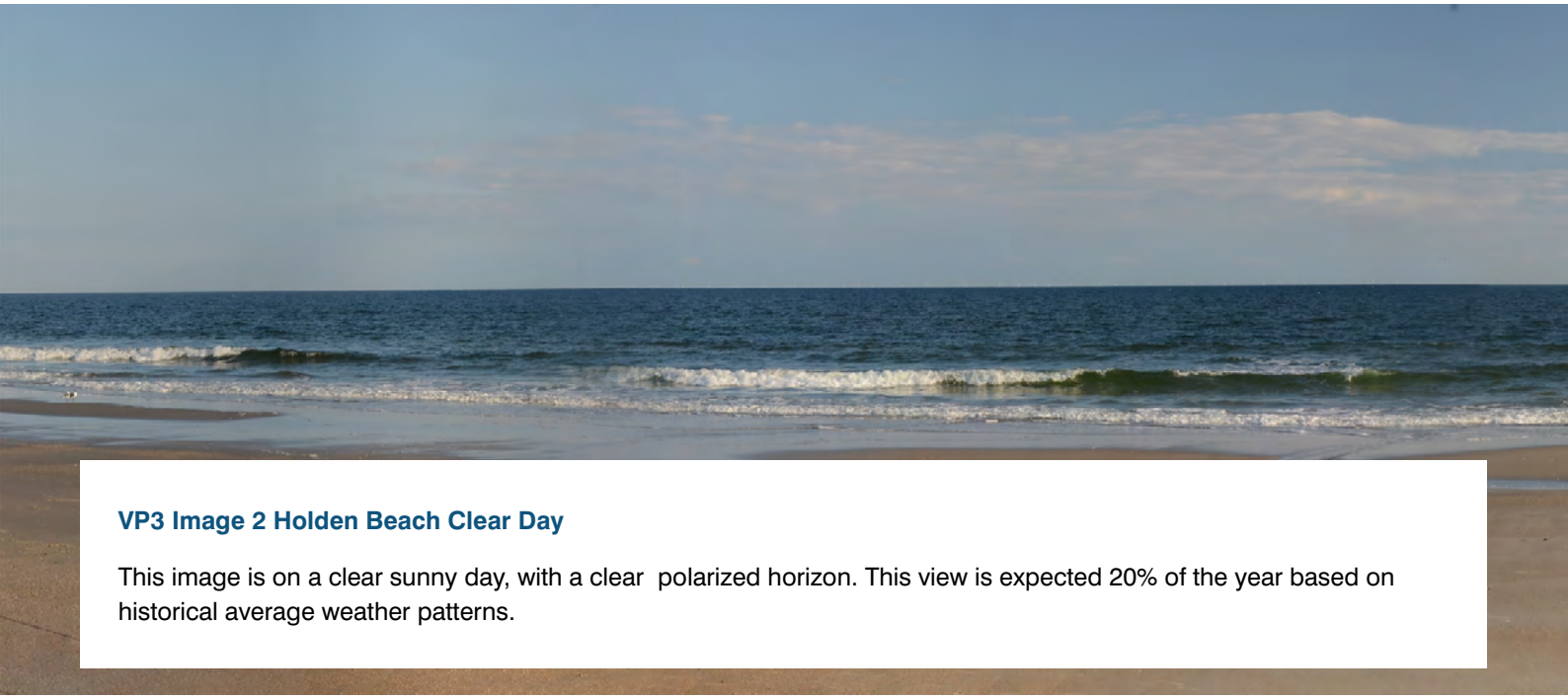

VP3 Image 2 Holden Beach Clear Day

This image is on a clear sunny day, with a clear polarized horizon. This view is expected 20% of the year based on historical average weather patterns.

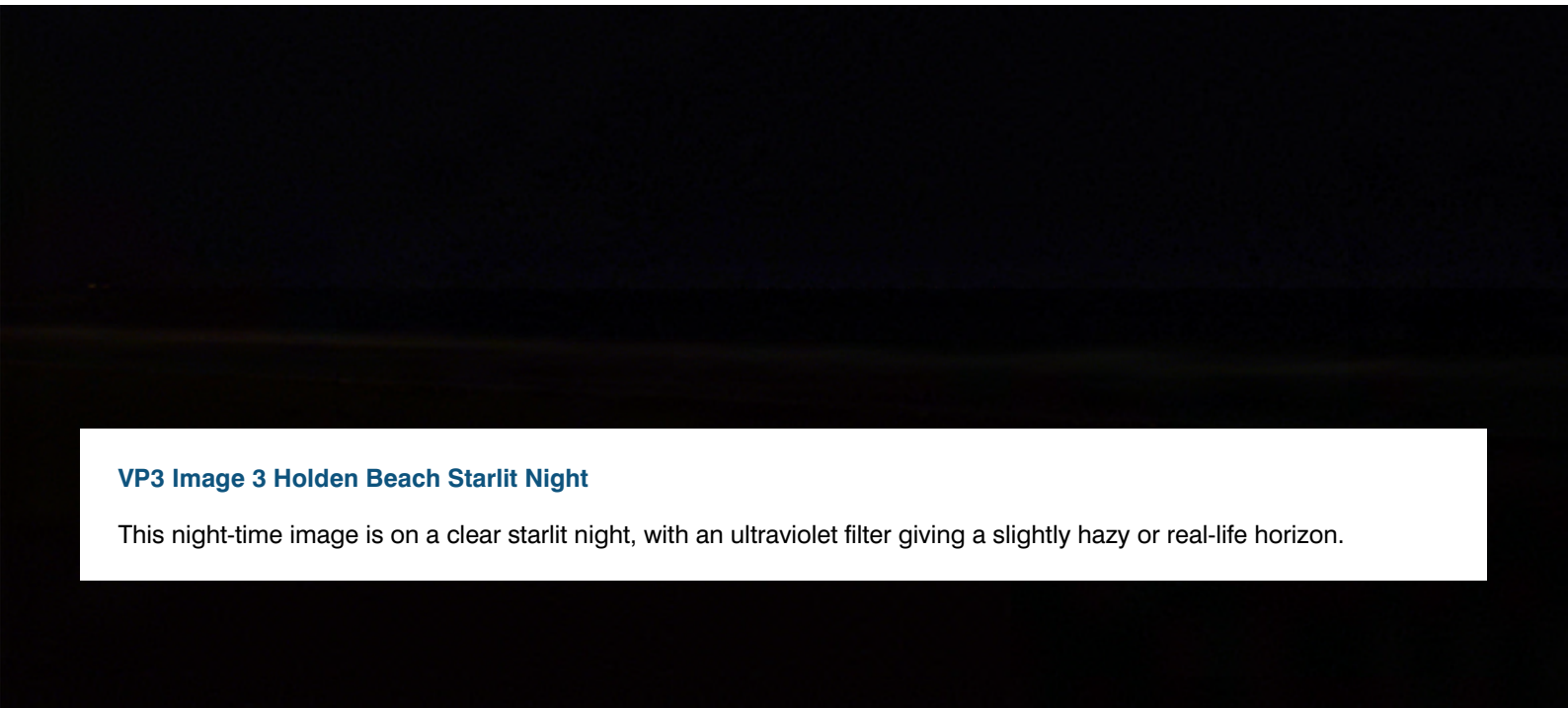

VP3 Image 3 Holden Beach Starlit Night

This night-time image is on a clear starlit night, with an ultraviolet filter giving a slightly hazy or real-life horizon.

APPENDICES

APPENDIX UNA *About Unasys*

About Unasys and their work in Offshore Wind

'In the last 10 years, the global growth in offshore wind has been significant and alongside the UK and EU, momentum in Ireland, and the USA is gathering pace.

With such growth comes complexity. The logistical challenges of installing arrays of turbines requires good definition, stringent planning, efficient generation of, access to, and management of complex data sets.

The Unasys Business function is built around the transfer of care, custody, and control of facilities throughout their key life cycle stages, Concept through Engineering, Construction, Commissioning, and Handover.

Founded in 2000, Unasys have helped deliver over 50 major complex energy projects across the globe.

Offshore renewables began for us with Sheringham shoal and then the balance of plant for Tees Offshore Wind. At about the same time, we began using digital twin technology on projects to complement our already established proprietary completions software. The technology would allow us to visualise and better understand the complexities of building and operating large infrastructure projects.

Digital twin technology is a critical means by which the life cycle phases from Concept to operation can be de-risked. Numerical experiments on farm orientation, maintenance interventions, crew transfer optimisations, inter-array cable routing, etc. allow scenario planning to be undertaken ahead of any firm investment or operational expenditure decisions being made.

The UK regulators were now taking an interest in this work and Unasys were asked to develop the Digital North Sea, on behalf of the UK and Scottish governments.

The Digital North Sea would provide asset visualisation including subsea infrastructure and seabed bathymetry. The Digital twinning of actual site characteristics, including asset visualisation, allows a repository of data to be generated for future quality assurance purposes. An overarching 2-tier platform to provide an interactive 3D representation of the North Sea Basin to all its underlying asset data.

For Offshore wind, a nascent industry, it is essential that as much as possible is done to facilitate strategic asset management from the outset'

Michael Flynn is a Chartered Engineer, Partner, and co-founder of Unasys.
He has worked in the Offshore Energy sector for over 30 years.

He was supported on the Wilmington East field area visualisation by Senior Data analyst, Dave Price Digital 3d modeller Ben Modica and Graphic Designer Alison Jackson-McGough.

APPENDIX I *Weather data and wind rose*

Location	(All)																	
Year	(All)																	
Count of WD	Column Labels																	
Row Labels	E	ENE	ESE	N	NE	NNE	NNW	NW	S	SE	SSE	SSW	SW	W	WNW	WSW	(blank)	Grand Total
<2 or (blank)	0.72%	0.70%	0.71%	0.79%	0.73%	0.66%	0.55%	0.56%	0.78%	0.70%	0.77%	0.84%	0.81%	0.68%	0.60%	0.75%	0.00%	11.34%
2-4	1.85%	2.12%	1.46%	2.06%	1.94%	1.83%	1.25%	1.27%	2.25%	1.21%	1.62%	3.51%	3.85%	2.10%	1.51%	3.09%	0.00%	32.96%
4-6	1.41%	2.38%	0.72%	2.42%	2.85%	2.74%	1.27%	1.13%	1.78%	0.63%	0.91%	2.98%	5.65%	1.95%	1.23%	4.04%	0.00%	34.08%
6-8	0.28%	0.88%	0.17%	1.51%	2.20%	2.14%	0.73%	0.60%	0.60%	0.21%	0.33%	0.87%	2.28%	0.90%	0.70%	1.76%	0.00%	16.17%
8-10	0.12%	0.16%	0.05%	0.43%	0.56%	0.58%	0.33%	0.23%	0.16%	0.06%	0.11%	0.18%	0.33%	0.35%	0.34%	0.36%	0.00%	4.32%
10-12	0.03%	0.04%	0.03%	0.07%	0.05%	0.12%	0.08%	0.04%	0.05%	0.02%	0.02%	0.07%	0.07%	0.09%	0.05%	0.06%	0.00%	0.88%
12-14	0.00%	0.00%	0.01%	0.02%	0.00%	0.04%	0.01%	0.01%	0.01%	0.01%	0.00%	0.01%	0.01%	0.01%	0.01%	0.01%	0.00%	0.14%
14-16	0.00%	0.00%	0.00%	0.00%	0.01%	0.02%	0.00%	0.01%	0.00%	0.00%	0.00%	0.00%	0.00%	0.00%	0.01%	0.00%	0.00%	0.07%
16-18	0.00%	0.00%	0.00%	0.00%	0.00%	0.00%	0.00%	0.01%	0.00%	0.00%	0.00%	0.00%	0.00%	0.00%	0.00%	0.00%	0.00%	0.03%
>18	0.00%	0.00%	0.00%	0.00%	0.00%	0.00%	0.00%	0.00%	0.00%	0.00%	0.00%	0.00%	0.00%	0.00%	0.00%	0.00%	0.00%	0.00%
Grand Total	**4.41%**	**6.29%**	**3.15%**	**7.30%**	**8.35%**	**8.12%**	**4.22%**	**3.86%**	**5.63%**	**2.84%**	**3.76%**	**8.46%**	**13.04%**	**6.06%**	**4.44%**	**10.07%**	**0.00%**	**100.00%**
Row Labels	E	ENE	ESE	N	NE	NNE	NNW	NW	S	SE	SSE	SSW	SW	W	WNW	WSW	(blank)	Grand Total
<2 or (blank)	0.007242905	0.006966877	0.007094625	0.007870244	0.007343279	0.006553974	0.005472671	0.00561857	0.007815494	0.007014782	0.007658089	0.00842002		0.006757003	0.006004197	0.00753034	0	0.113447851
2-4	0.018493932	0.021233689	0.014597591	0.020576695	0.019426955	0.018313715	0.012503422	0.012713295	0.022479241	0.012145269	0.016185327	0.035121818		0.020971348	0.015058396	0.030947167	0	0.329637741
4-6	0.014102564	0.023820604	0.007185875	0.024197007	0.028533625	0.027406698	0.012660827	0.011292089	0.017814125	0.00626882	0.009079296	0.029772333		0.019534173	0.012257049	0.04039374	0	0.340834018
6-8	0.002824163	0.008803267	0.001694954	0.015065243	0.022004745	0.021418469	0.007318186	0.006036135	0.005983666	0.002091888	0.00330094	0.00871658		0.008988046	0.00701022	0.017588284	0	0.161677617
8-10	0.00116799	0.001644767	0.000469933	0.004336618	0.005595857	0.005757825	0.003275846	0.002265261	0.001596861	0.00061137	0.00109499	0.001781641		0.00333744	0.00337622	0.003592937	0	0.043217903
10-12	0.00029656	0.000337184	0.000305685	0.0007949	0.000458527	0.001154302	0.000348518	0.000406059	0.000515558	0.000182498	0.000246373	0.000652432	0.00068665	0.000917054	0.000469933	0.000590839	0	0.008807829
12-14	4.56246E-06	2.73748E-05	9.12492E-05	0.000155124	2.9656E-05	0.000359559	6.15932E-05	5.24683E-05	9.12492E-05	0.000107218	1.82498E-05	0.000100374	9.12492E-05	6.61557E-05	5.01871E-05	6.15932E-05	0	0.001377863
14-16	2.28123E-06	9.12492E-06	2.50935E-05	4.56246E-05	5.24683E-05	0.000218998	1.36874E-05	7.98431E-05	4.56246E-06	1.36874E-05	3.64997E-05	2.28123E-05	4.56246E-05	2.05311E-05	0.00011178	0	0	0.000702619
16-18	0	0	0	2.28123E-05	9.12492E-06	3.64997E-05	2.73748E-05	0.000116343	4.56246E-06	0	1.14062E-05	6.84369E-06	4.56246E-06	6.84369E-06	4.56246E-05	0	0	0.000291997
>18	0	0	0	0	0	2.28123E-06	0	2.28123E-06	0	0	0	0	0	0	0	0	0	4.56246E-06
Grand Total	**0.044134958**	**0.063**	**0.031**	**0.072974268**	**0.083**	**0.081**	**0.042**	**0.038582444**	**0.056**	**0.028**	**0.037**	**0.084**	**0.130**	**0.060**	**0.044**	**0.1007**	**0**	**1**
Row Labels	N	NNE	NE	ENE	E	ESE	SE	SSE	S	SSW	SW	WSW	W	WNW	NW	NNW		
<2 mph	1%	1%	1%	1%	1%	1%	1%	1%	1%	1%	1%	1%	1%	1%	1%	1%	11%	
2-4 mph	3%	2%	3%	3%	3%	2%	2%	2%	3%	4%	5%	4%	3%	2%	2%	2%	44%	
4-6 mph	5%	5%	6%	5%	4%	3%	3%	3%	5%	7%	10%	8%	5%	3%	3%	3%	78%	
6-8 mph	7%	7%	8%	6%	4%	3%	3%	4%	5%	8%	13%	10%	6%	4%	4%	4%	95%	
8-10 mph	7%	8%	8%	6%	4%	3%	3%	4%	6%	8%	13%	10%	6%	4%	4%	4%	99%	
10-12 mph	7%	8%	8%	6%	4%	3%	3%	4%	6%	8%	13%	10%	6%	4%	4%	4%	100%	
12-14 mph	7%	8%	8%	6%	4%	3%	3%	4%	6%	8%	13%	10%	6%	4%	4%	4%	100%	
14-16 mph	7%	8%	8%	6%	4%	3%	3%	4%	6%	8%	13%	10%	6%	4%	4%	4%	100%	
16-18 mph	7%	8%	8%	6%	4%	3%	3%	4%	6%	8%	13%	10%	6%	4%	4%	4%	100%	
>18 mph	7%	8%	8%	6%	4%	3%	3%	4%	6%	8%	13%	10%	6%	4%	4%	4%	100%	

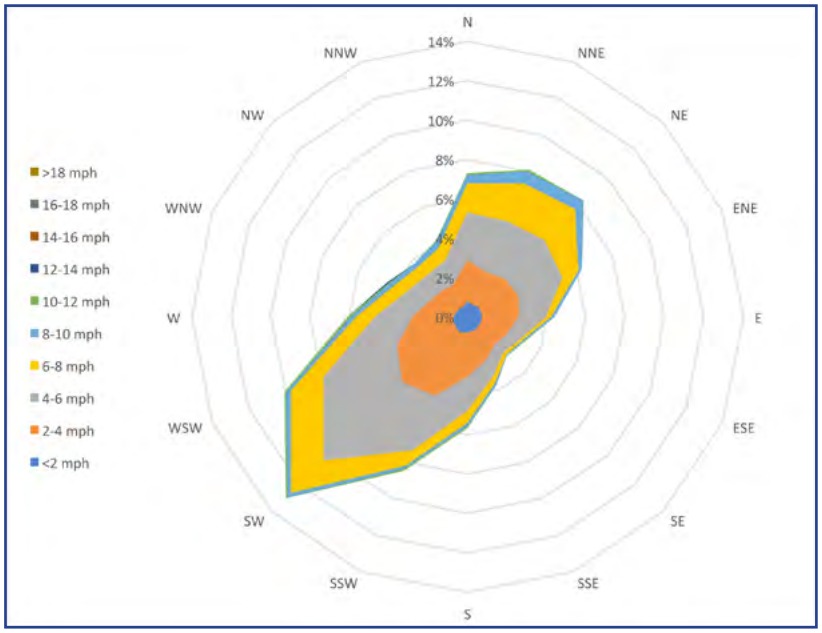

APPENDIX II *Investigation into wind turbine layout*

LES investigation of infinite staggered wind-turbine arrays

LES investigation of infinite staggered wind-turbine arrays

Xiaolei Yang and Fotis Sotiropoulos[1]

St. Anthony Falls Laboratory, Department of Civil Engineering, University of Minnesota, 2 Third Avenue SE, Minneapolis, MN 55414, USA
[1] Corresponding author: fotis@umn.edu

Abstract. The layouts of turbines affect the turbine wake interactions and thus the wind farm performance. The wake interactions in infinite staggered wind-turbine arrays are investigated and compared with infinite aligned turbine arrays in this paper. From the numerical results we identify three types of wake behaviours, which are significantly different from wakes in aligned wind-turbine arrays. For the first type, each turbine wake interferes with the pair of staggered downstream turbine wakes and the aligned downstream turbine. For the second type, each turbine wake interacts with the first two downstream turbine wakes but does not show significant interference with the second aligned downstream turbine. For the third type, each turbine wake recovers immediately after passing through the gap of the first two downstream turbines and has little interaction with the second downstream turbine wakes The extracted power density and power efficiency are also studied and compared with aligned wind-turbine arrays.

1. Introduction

In wind farms the wakes from upstream turbines affect the power extraction and dynamic loadings of the downstream turbines. This influence depends on the layout of wind turbines, wind directions and many other effects. In comparison with aligned turbine arrays, the turbine wakes are affected by the so-called venturi effects [1] in staggered turbine arrays. The far-wake region of an upstream turbine also interacts with the near wake region of its downstream turbine side by side. How these different wake interactions affect the wake behaviours and power extraction in infinite large staggered wind-turbine arrays will be investigated in this paper using large-eddy simulation with turbines parametrized as actuator disks.

Most previous numerical studies have focused either on wakes of a single stand-alone wind turbine or aligned wind-turbine arrays. For instance, the turbulence characteristics of a single wind turbine wake was studied by Jimenez et al. [2, 3] while turbine spacing effects in infinite aligned wind-turbine arrays were investigated by Calaf et al. [4] and Yang et al. [5]. To the best of our knowledge, the only numerical work on finite staggered wind farms was reported by Ammara et al. [1] by using Reynolds-averaged Navier-Stokes equation with an actuator disk model.

Wind tunnel experiments have also been used to investigate wind turbine wakes. However, it is difficult to mimic infinite large wind-turbine arrays in a wind tunnel experiment because of the limits imposed by the wind tunnel and the inherent side-wall effects. The wake behind a single turbine was investigated by Chamorro and Porté-Agel [6]. Studies on aligned wind-turbine

arrays can be found in the work by Cal et al. [7] and Chamorro and Porté-Agel [8]. Staggered wind-turbines arrays were investigated by Chamorro et al. [9].

2. Numerical methods

2.1. Governing equations

The LES equations governing the incompressible turbulent flows are the 3D, unsteady, filtered continuity and Navier-Stokes equations. The curvilinear immersed boundary (CURVIB) method [10] is used to solve these equations in order to facilitate future extension of the method to simulate topography effects. In this method the governing equations are first written in Cartesian coordinates x_i and then transformed fully (both the velocity vector and spatial coordinates are expressed in curvilinear coordinates) in non-orthogonal, generalized, curvilinear coordinates ξ^i. The transformed equations read in compact tensor notation (repeated indices imply summation) as follows $(i, j = 1, 2, 3)$:

$$J\frac{\partial U^j}{\partial \xi^j} = 0, \tag{1}$$

$$\begin{aligned}\frac{1}{J}\frac{\partial U^i}{\partial t} =& \frac{\xi_l^i}{J}\left(-\frac{\partial}{\partial \xi^j}(U^j u_l) + \frac{\mu}{\rho}\frac{\partial}{\partial \xi^j}\left(\frac{g^{jk}}{J}\frac{\partial u_l}{\partial \xi^k}\right)\right.\\ &\left.-\frac{1}{\rho}\frac{\partial}{\partial \xi^j}(\frac{\xi_l^j p}{J}) - \frac{1}{\rho}\frac{\partial \tau_{lj}}{\partial \xi^j} + f_i\right),\end{aligned} \tag{2}$$

where $\xi_l^i = \partial\xi^i/\partial x_l$ are the transformation metrics, J is the Jacobian of the geometric transformation, u_i is the i^{th} component of the velocity vector in Cartesian coordinates, $U^i{=}(\xi_m^i/J)u_m$ is the contravariant volume flux, $g^{jk} = \xi_l^j\xi_l^k$ are the components of the contravariant metric tensor, ρ is the density, μ is the dynamic viscosity, p is the pressure, $f_i(i = 1, 2, 3)$ are the body forces introduced by the wind turbines and τ_{ij} represents the anisotropic part of the subgrid scale stress tensor, which is modelled by the eddy-viscosity subgrid scale model [11]. For details of the CURVIB method and numerical schemes, please refer to the papers [10, 12].

2.2. Actuator disk model

In the actuator disk model a wind turbine rotor is represented by a permeable circular disk that is discretized using an unstructured triangular grid. Drag forces exerted by the turbine rotor on wind are uniformly distributed over the disk surface to model the momentum extraction by a turbine rotor. The thrust force on the wind turbine rotor is calculated from the following expression

$$F_T = \frac{1}{2}\rho C_T U_\infty^2 \frac{\pi}{4}D^2, \tag{3}$$

where ρ is the air density, C_T is the thrust coefficient, U_∞ is the incoming velocity and D is the diameter of wind turbine rotor. In the present work, the C_T is determined from the one-dimensional momentum theory [13] and reads as

$$C_T = 4a(1-a), \tag{4}$$

where a is the axial induction factor of the turbine rotor, which is specified in our simulations. The incoming velocity U_∞ for a wind turbine in an infinite wind-turbine array is calculated using the relation from one-dimensional momentum theory:

$$U_\infty = u_d/(1-a). \tag{5}$$

In the above equation u_d is the disk-averaged streamwise velocity on the actuator disk.

Generally, the positions of grid nodes of the actuator disk do not coincide with those of the background (fluid) domain. Quantities are transferred between the two grids through discrete delta functions. The velocities on the disk are interpolated from the background grid by:

$$u_i(\mathbf{X}) = \sum_{g_f} u_i(\mathbf{x})\, \delta_h(\mathbf{x} - \mathbf{X}) V(\mathbf{x}), \tag{6}$$

where $\mathbf{x}$ and $\mathbf{X}$ denote the coordinates of the meshes for fluid and actuator disks, respectively, g_f represents the collection of background grid cells, δ_h is the discrete delta function and $V(\mathbf{x})$ is the volume of the background cell. The forces on the background grid nodes are distributed from the grid nodes of actuator disks by the expression shown as follows:

$$f_i(\mathbf{x}) = \sum_{g_t} f_i(\mathbf{X}) \delta_h(\mathbf{x} - \mathbf{X}) A(\mathbf{X}), \tag{7}$$

where g_t represents the collection of actuator disk cells and $A(\mathbf{X})$ is the area of actuator disk cell. In the present work a smoothed discrete delta function proposed by Yang et al. [14] was used.

2.3. Boundary conditions

In all simulations, periodic boundary conditions are used in the horizontal directions. A free-slip boundary condition is used at the top boundary and a wall model is used at the bottom boundary. A mean pressure gradient is applied in the streamwise direction to ensure a constant mass flow rate. At the bottom boundary, the shear stress boundary condition and no-flux boundary condition are used for the wall-parallel and wall-normal velocity components, respectively. The wall shear stress is calculated from the logarithmic law for rough wall [15], which is given as follows:

$$\frac{U}{u_*} = \frac{1}{\kappa} \ln \frac{z}{z_{0,lo}}, \tag{8}$$

where U is the mean wall-parallel velocity and $z_{0,lo}$ is the roughness height of the land surface. In the present work, the magnitude of the instantaneous parallel velocity U_2 at the second off-wall grid node is used for calculating u_* from the Eq (8), which is calculated as follows:

$$U_2 = \sqrt{u_2^2 + v_2^2}, \tag{9}$$

where u_2 and v_2 are the instantaneous steamwise and spanwise velocity components at the second off-wall grid node, respectively.

3. Numerical results

Four infinite staggered wind-turbine arrays together with two infinite aligned arrays are simulated to study the effects of turbine layout and spacing on the wake behaviour and power extraction of infinite wind farms. In all cases, the area of the land is fixed and is set equal to $30D$ and $20D$ in the streamwise and spanwise directions, respectively. For the staggered cases, the number of rows of wind turbines in the streamwise direction ($N_{t,x}$) is fixed at 4. The number of turbines in each row ($N_{t,y}$) is varied to be 3, 4, 5 and 6 for the four staggered cases, respectively. The simulated layout of a staggered wind farm is demonstrated in Figure 1, which shows a specific layout with 4 rows of wind turbine in the streamwise direction and 5 turbines in each row. The two aligned wind farm cases are simulated in order to compare with the corresponding staggered case with 5 turbines in each row. The two aligned cases consist of: 1)

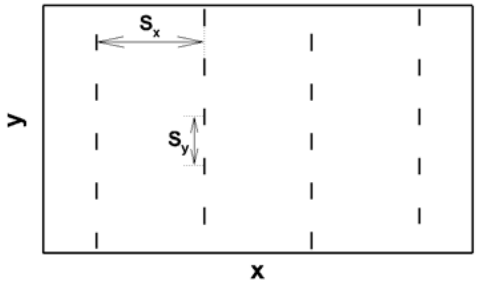

Figure 1: Schematic of staggered wind-turbine array. The turbines are represented by solid segments and S_x and S_y denote the turbine spacings in streamwise and spanwise directions, respectively.

4 rows in the streamwise direction with 5 turbines in each row; and 2) 2 rows with 10 turbines in each row. For all cases, the hub height of the wind turbine $z_h = D$ and the domain size in the vertical direction $H = 10D$. The computational grid consists of 200, 150 and 128 grid nodes in the streamwise, spanwise and vertical directions, respectively. The effect of viscous terms is neglected because of the very high Reynolds number of the atmospheric boundary layer. The roughness height of the land $z_{0,lo} = 10^{-4}H$. The induction factor $a = 0.25$. In the following discussions, we will denote the sets of cases by "S $N_{t,x}$-$N_{t,y}$" and "A $N_{t,x}$-$N_{t,y}$" for staggered and aligned layouts, respectively.

In order to facilitate the physical interpretation of our results, the velocity field is normalized by the equivalent geostrophic velocity G, which is calculated from the geostrophic drag law [16],

$$\frac{G}{u_*} = \sqrt{A^2 + \left(\frac{1}{\kappa}\ln\frac{u_*}{f z_{0,hi}} - C\right)^2}, \tag{10}$$

where the Coriolis parameter $f = 2\Omega\sin\theta$ is set equal to $1 \times 10^{-4}s^{-1}$ (where Ω is the angular speed of the earth and latitude $\theta = 40^o$), $A = 11.25$, $C = 4.5$, and $z_{0,hi}$ is the effective roughness height of the wind farm covered land. The total friction velocity u_* in the above equation is provided by LES and the effective roughness height is calculated by using the mean streamwise velocity at $z = 0.175H$ via Eq. (8).

In Figure 2, we show the contours of instantaneous streamwise velocity on the x-y plane positioned at hub height. As seen, the flow fields for all cases exhibit high speed streaks, low speed wakes and wake meandering. While at first glance the general behaviour of staggered and aligned wakes are nearly the same, significant differences are observed in the structure of the high speed streaks. For the case A4-5 the high speed streaks are elongated spanning the entire gap between adjacent columns of turbines. For the case A2-10, however, the high speed streaks are only located within the gaps between turbine columns in the near wake and merge with each other in the far wake. The high speed streaks behave significantly different for the staggered cases in which the high speed streaks usually cross different columns of turbines and slow down locally because of the momentum extraction by turbines.

Figure 3 shows the mean flow field for each case, averaged in time and in space (every 2 staggered turbines for staggered arrays and every turbine for aligned arrays). For staggered arrays we observe three different types of wake behavior. For the first type, each turbine wake interferes with the pair of staggered downstream turbine wakes and the aligned downstream turbine (Figures 3a and 3b). For the second type, each turbine wake interacts with the first two downstream turbine wakes but does not show significant interference with the second aligned downstream turbine (Figure 3c). For the third type (Figure 3d), each turbine wake recovers

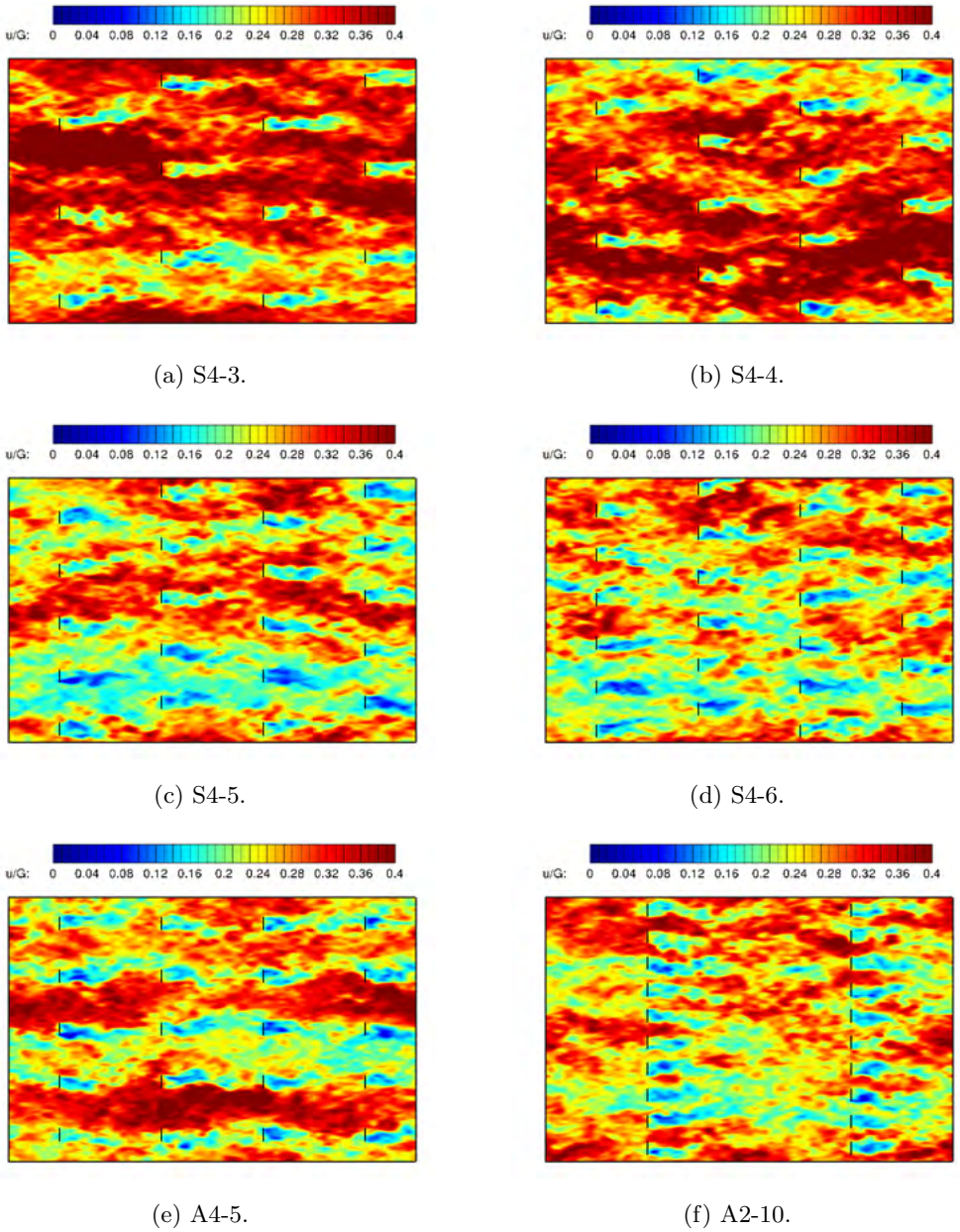

(a) S4-3. (b) S4-4.

(c) S4-5. (d) S4-6.

(e) A4-5. (f) A2-10.

Figure 2: Contours of instantaneous streamwise velocity on the x-y plane at the hub height normalized by G for staggered (a through d) and aligned (e and f) wind farms.

immediately after passing through the gap of the first two downstream turbines and has little interaction with the second downstream turbine wakes. Comparing the wakes for the S4-5 and A4-5 and A2-10 cases, we observe that the wake recovery is more significant for the S4-5 and A2-10 layouts before the wake encounters the next row of immediately downstream wind turbines. However, the mechanism for wake recovery is quite different. For the A2-10 layout, the wake recovers only because of the streamwise turbine spacing. For the S4-5 layout, however, there are two factors affecting wake recovery: the streamwise turbine spacing and the acceleration effect caused by the first two downstream turbines, an effect which increases with decreasing the spanwise turbine spacing for current cases.

In Figure 4, we show the mean streamwise velocity profiles averaged in time and horizontal

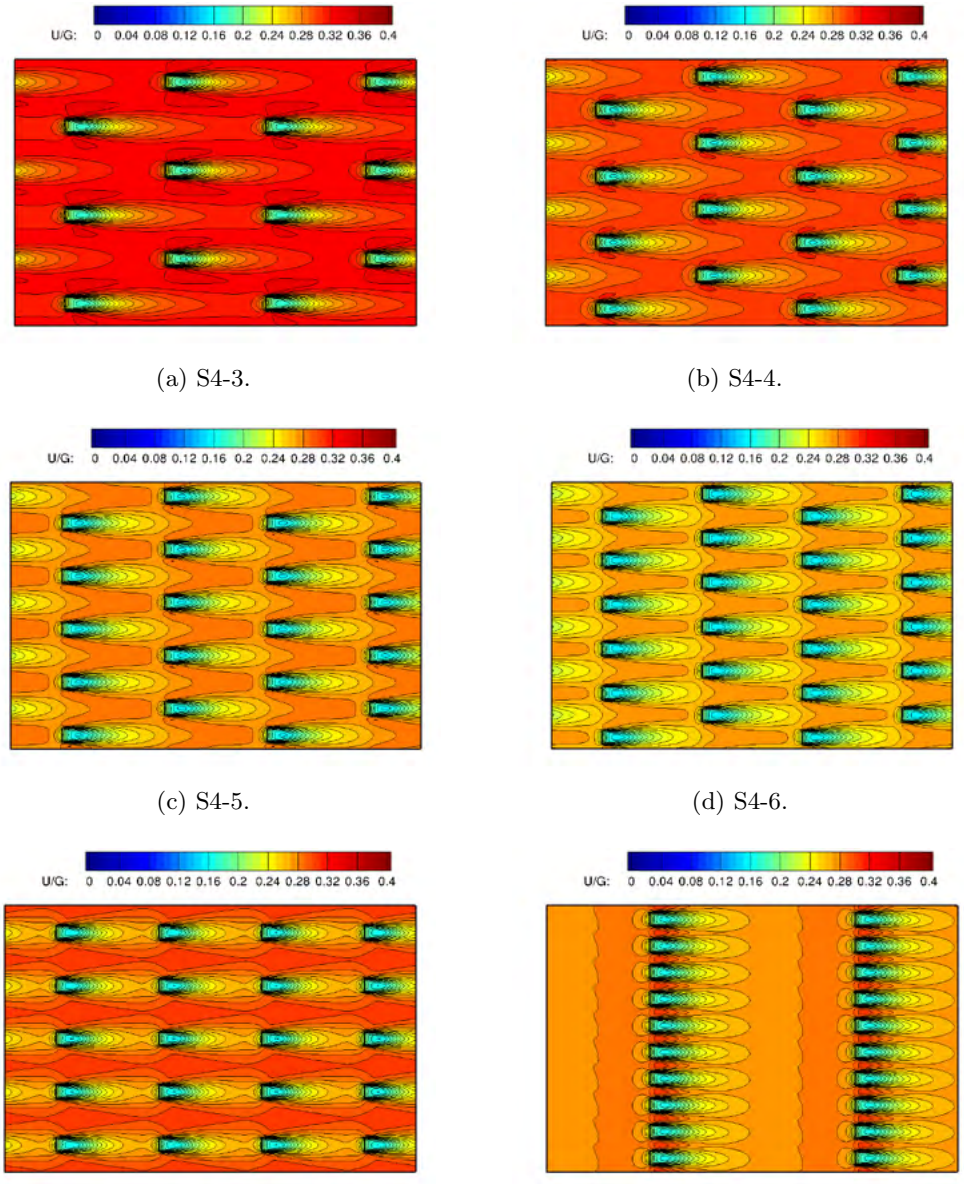

(a) S4-3. (b) S4-4.

(c) S4-5. (d) S4-6.

(e) A4-5. (f) A2-10.

Figure 3: Contours of mean streamwise velocity on the x-y plane at the hub height normalized by G for staggered (a through d) and aligned (e and f) wind farms.

directions. As seen in Figure 4a, the two logarithmic layers known to form for aligned wind farms (Calaf et al. [4], Yang et al. [5]) also exist for the staggered wind farms. In Figure 4b, we compare mean velocity profiles for staggered and aligned cases. It is seen that the three profiles are nearly collapsed with each other for the outer logarithmic layer ($z > z_h$). For the inner part, the profile from case A4-5 is shifted upwards compared to the profiles from the other two cases, which are nearly identical in the lower part.

Let finally investigate the effect of turbine spacing on the extracted power. Figure 5a shows the extracted power density for all simulated cases as a function of N_t ($N_t = N_{t,x} \times N_{t,y}$), which

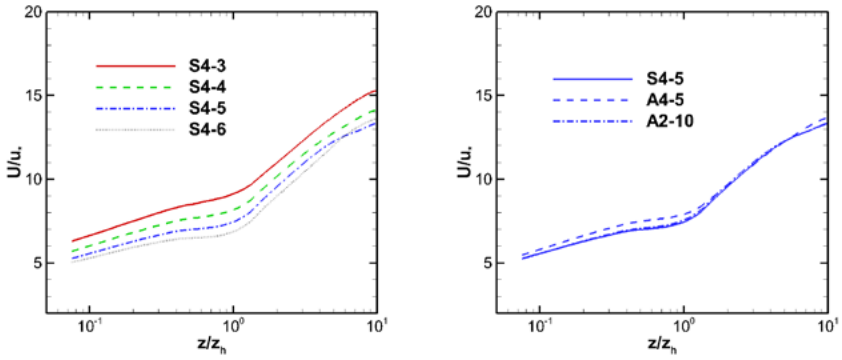

(a) Staggered cases. (b) Staggered case vs. aligned cases.

Figure 4: Mean streamwise velocity profiles.

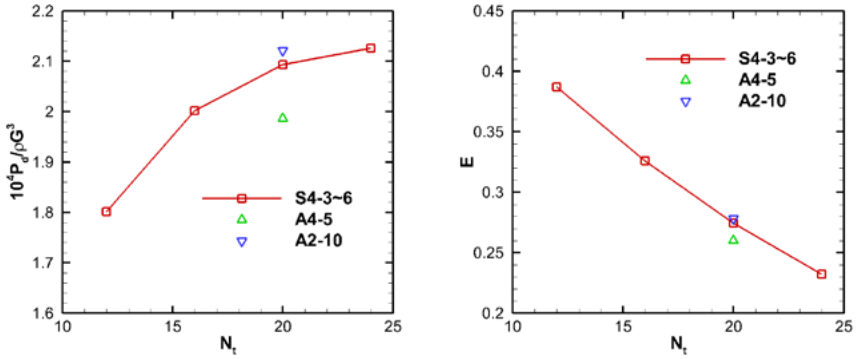

(a) Extracted power density. (b) Extracted power efficiency.

Figure 5: Extracted power density and power efficiency.

is defined as follows:

$$P_d \equiv \frac{P}{S_x S_y}, \tag{11}$$

where P is the extracted power averaged over all turbines. It is seen that the extracted power density increases with increasing the number of turbines. For the same number of wind turbine ($N_t = 20$), the case A2-10 is able to extract somewhat higher power density than that from the staggered case S4-5. While the case A4-5 gives much lower power density than the corresponding staggered case. Figure 5b shows the extracted power efficiency, which is defined as follows:

$$E \equiv P/P_{1tb}, \tag{12}$$

where P_{1tb} is the power that would be extracted from a single stand-alone wind turbine under the same geostrophic wind speed and land surface roughness. It is seen that the extracted power efficiency decreases with increasing the number of turbines in each row. Similar to the power density, the efficiency from the cases A2-10 and A4-5 is somewhat higher and lower, respectively, than that for the S4-5 case.

4. Summary

In this paper, we investigate the wake behaviour of infinite staggered wind-turbine arrays by carrying out four cases with different spanwise turbine spacings at the same streamwise turbine spacing together with the other two aligned cases. In aligned turbine arrays, the wake recovery mainly depends on the size of the streamwise turbine spacing. In staggered turbine arrays, acceleration (venturi) effect caused by the first two downstream turbines also plays an important role in wake recovery besides of the streamwise turbine spacing. Based on how one turbine wake interacts with its downstream turbine wakes, three different wake patterns are identified for staggered turbine arrays.

For a given turbine occupied area, staggered turbine layout is preferred for locations without a fixed prevailing wind direction. An aligned turbine array with a longer streamwise turbine spacing, on the other hand, is suitable for locations with a fixed prevailing wind direction.

Acknowledgments

This work was supported by Department of Energy DOE (DE-EE0002980) and Xcel Energy through the Renewable Development Fund (grant RD3-42). Computational resources were provided by the University of Minnesota Supercomputing Institute.

References

[1] Ammara I, Leclerc C and Masson C 2002 *J. Sol. Energy Eng.* **124** 345–356
[2] Jimenez A, Crespo A, Migoya E and Garcia J 2007 *Journal of Physics: Conference Series* **75** 012041
[3] Jimenez A, Crespo A, Migoya E and Garcia J 2008 *Environ. Res. Lett.* **3** 015004
[4] Calaf M, Meneveau C and Meyers J 2010 *Phys. Fluids* **22** 015110
[5] Yang X, Kang S and Sotiropoulos F 2012 *Physics of Fluids (1994-present)* **24** 115107
[6] Chamorro L P and Porté-Agel F 2009 *Boundary-Layer Meteorol.* **132** 129–149
[7] Cal R B, Lebrón J, Castillo L, Kang H S and Meneveau C 2010 *J. Renewable Sustainable Energy* **2** 013106
[8] Chamorro L P and Porté-Agel F 2011 *Energies* **4** 1–22
[9] Chamorro L P, Arndt R E A and Sotiropoulos F 2011 *Boundary-Layer Meteorol.*
[10] Ge L and Sotiropoulos F 2007 *J. Comput. Phys.* **225** 1782–1809
[11] Germano M, Piomelli U, Moin P and Cabot W H 1991 *Phys. Fluids A* **3** 1760–1765
[12] Kang S, Lightbody A, Hill C and Sotiropoulos F 2011 *Adv. Water Resour.* **34** 98–113
[13] Hansen M O L 2000 *Aerodynamics of wind turbines* (James & James (Science Publishers) Ltd)
[14] Yang X, Zhang X, Li Z and He G W 2009 *J. Comput. Phys.* **228** 7821–7836
[15] Jiménez J 2004 *Annu. Rev. Fluid Mech.* **36** 173–196
[16] Tennekes H and Lumley J L 1972 *A First Course in Turbulence* (MIT Press, Cambridge, MA)

APPENDIX III *Wind turbine specification*

The 13 MW Wind Turbine Generators proposed for Wilmington East Offshore Wind Area

https://www.ge.com/renewableenergy/wind-energy/offshore-wind/haliade-x-offshore- turbine

Haliade-X wind turbine technical specifications

Haliade-X	12 MW	13 MW	14 MW
Output (MW)	12	13	14
Rotor diameter (m)	220	220	220
Total height (m)	up to 260	up to 260	up to 260
Frequency (Hz)	50 & 60	50 & 60	50 & 60
Gross AEP (GWh)	~68	~71	~74
Capacity Factor (%)	63	60-64%	60-64%
IEC Wind Class	IB	IC	IC

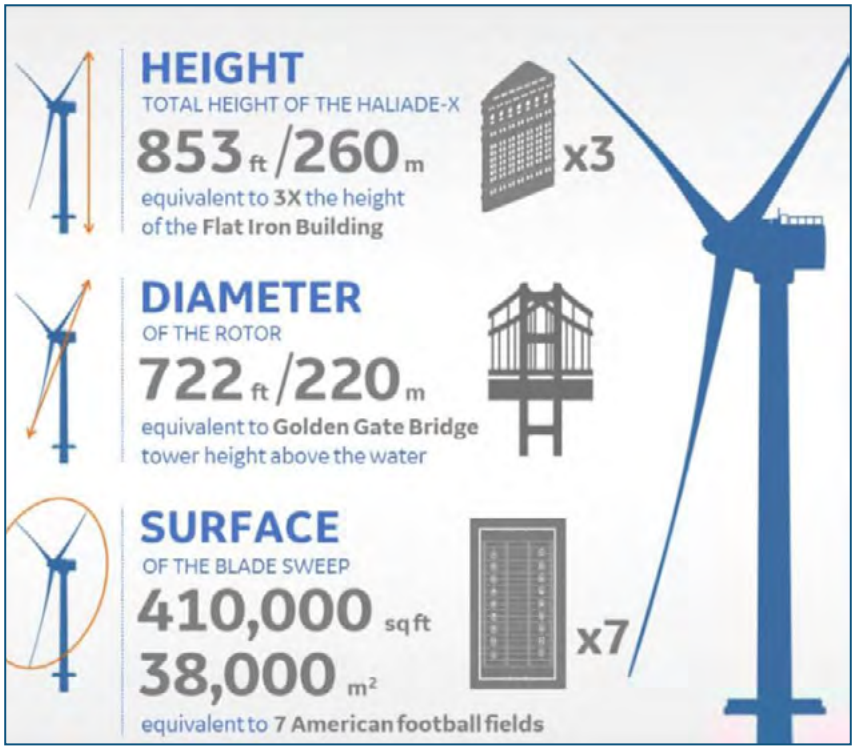

APPENDIX IV *Distance to horizon*

Distance to horizon

1) To calculate how much of a distant object is visible above the horizon. Observer's eye is **10 metres above sea level**

   Assume 10M is the view from a balcony overlooking a beach, and using the formula below, The formula for calculating the horizon at 10M above sea level is

   $3.57\sqrt{10}$

   3.57 * 3.16 = 11.28 KM = **6.1 nautical miles. This is the distance to the horizon at 10M**

   The nearest wind turbine from Bald head Island however is 17 nm
   (17 nm – 6.1nm) = 8.9 nautical miles further away than the horizon, or a further 16.5KM.

a) To calculate the height (h) in Metres of the point of the wind turbine that is just visible at 17nm (i.e., From **Bald Head Island**)

   h = (16.5/3.57) squared

   h = 4.62 squared

   h = 21.3 M

   Therefore, at 17nm, and at 10M above sea level, only the WTG above 21.3M is visible

b) To calculate the height (h) in Metres of the point of the wind turbine that is just visible at 22nm (i.e., From **Oak Beach**)

   22nm - 6.1nm = 13.9 nm or 25.7KM

   h = (25.7/3.57) squared

   h = 7,19 squared

   h = 51.82 M

   Therefore, at 22nm, and at 10M above sea level, only the WTG above 51.82M is visible.

c) To calculate the height (h) in Metres of the point of the wind turbine that is just visible at 38.25 nm, or the furthest point from **Oak Beach**

   38.25 – 6.1 = 32.15 nm or 59.5 KM

   h = (59.5/3.57) squared

   h = 16.7 squared

   h = 278 M

Therefore, at 38.25 nm, and at 10M above sea level, only the WTG above 278 M is visible.

2) To calculate how much of a distant object is visible above the horizon. Observer's eye is **2 metres above sea level**

   Assume 2M is the view from a beach, and using the formula below,
   The formula for calculating the horizon at 2M above sea level is

   3.57* Square root of 2M

   3.57 * 1.41 = 5,1 KM = **2.8 nautical miles. This is the distance to the horizon at 2M**

   The nearest wind turbine from Bald head Island however is 17 nm
   (17 nm – 2.8 nm) = 14.2 nautical miles further away than the horizon, or a further 26.3KM.

a) To calculate the height (h) in Metres of the point of the wind turbine that is just visible at 17nm (i.e., From **Bald Head Island**)

   h = (26.3/3.57) squared

   h = 7.4 squared

   h = 54.2 M

   Therefore, at 17nm, and at 2M above sea level, only the WTG above 54.2M is visible

b) The furthest wind turbine from Bald head Island however is
   (31.77 nm – 2.8 nm) = 29 nautical miles further away than the horizon, or a further 53.7KM.

   To calculate the height (h) in Metres of the point of the wind turbine that is just visible at 17nm (i.e., From **Bald Head Island**)

   h = (53.7/3.57) squared

   h = 15.04 squared

   h = 226 M

   Therefore, at 17nm, and at 2M above sea level, only the WTG above 226 M is visible

References

https://en.wikipedia.org/wiki/Horizon

10KM = 5.4 nautical miles

APPENDIX V *Wind farm viewing gradient*

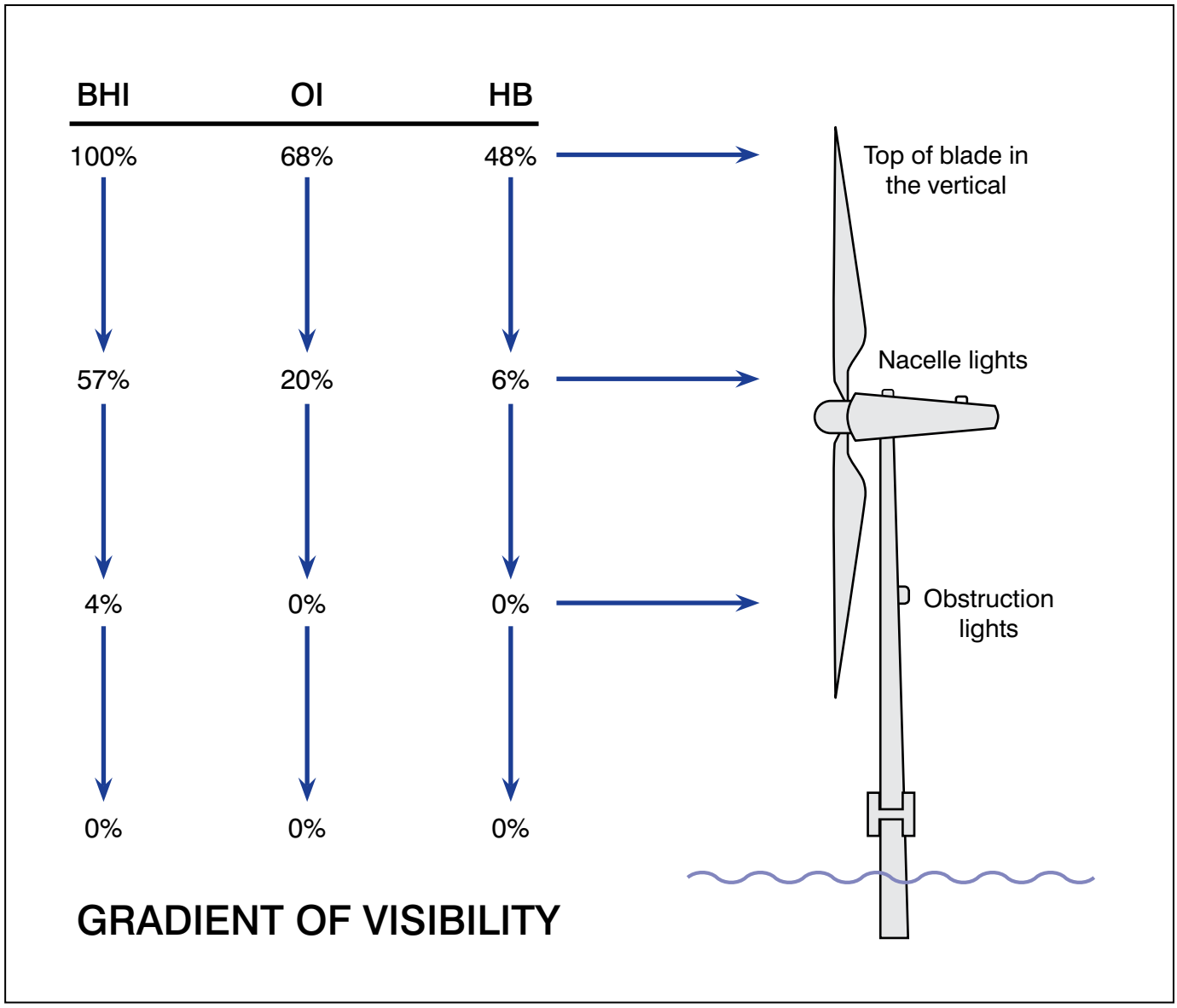

APPENDIX VI *Prevailing wind*

The prevailing wind

It was important for us to understand if the Wilmington East offshore area had a prevailing wind as this would help determine the proposed layout of the turbines in the field.

As can be seen in **the image** below, there is a prevailing wind for Offshore North Carolina, and it is **South Westerly**.

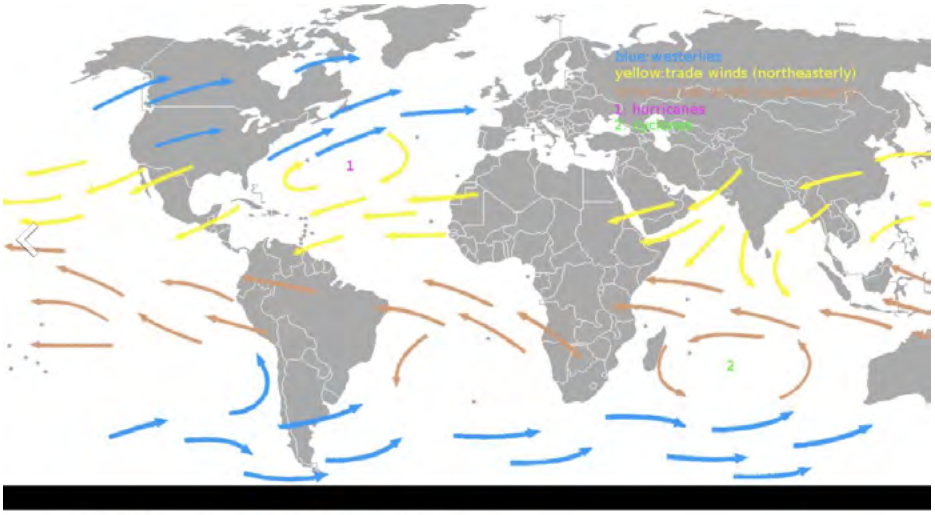

The westerlies (blue) and trade winds (yellow and brown)

https://en.wikipedia.org/wiki/Prevailing_winds#/media/File:Map_prevailing_winds_on_earth.png

Weather data and Wind rose

Unasys also engaged with https://customweather.com/ in the USA, to source the last ten years weather data for the Wilmington East area. See appendix i

The 10-year wind data would enable us to develop the **wind rose** for the Wilmington East field.

A **wind rose** is a graphic tool used by meteorologists to give a succinct view of how wind speed and direction are typically distributed at a particular location. Presented in a polar coordinate grid, the wind rose shows the frequency of winds blowing from a particular direction. The length of each spoke around the circle is related to the proportion of the time that the wind blows from each direction.

The Windrose for the Wilmington East Field

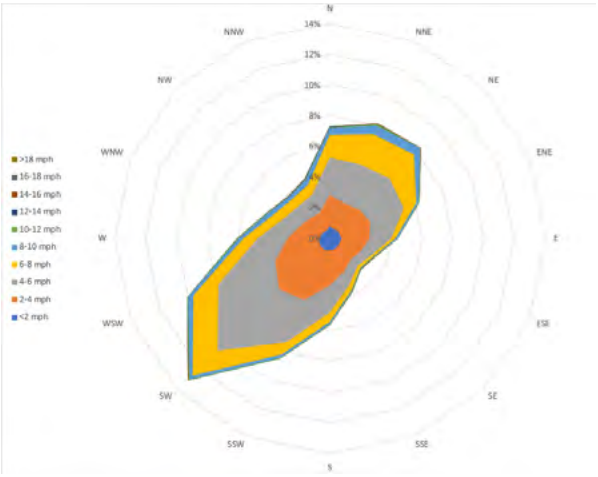

The wind rose validates the prevailing wind as South Westerly which will be key laying out the Wind Turbine Generators in the Field.

The data used to determine the wind rose was taken at 90M above sea level, or roughly at the hub height or Rotor centre

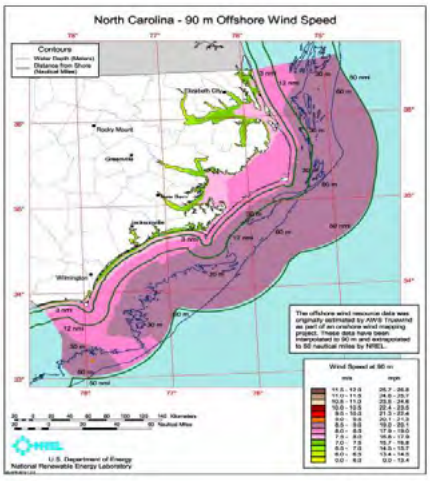

APPENDIX VII *Layout of the wind farm*

Layout of the wind farm

The prevailing wind in the East Wilmington field is south Westerly. This information will now help to determine the layout of the Wind Turbine Generators, within the Wilmington East area.

From the publication:

The Science of Making Torque from Wind 2012 IOP Publishing. Journal of Physics: Conference Series 555 (2014) 012109 doi:10.1088/1742-6596/555/1/012109
See appendix ii

The following Summary is made:

'In this paper, we investigate the wake behaviour of infinite staggered wind-turbine arrays by carrying out four cases with different spanwise turbine spacings at the same streamwise turbine spacing together with the other two aligned cases. In aligned turbine arrays, the wake recovery mainly depends on the size of the streamwise turbine spacing.

In staggered turbine arrays, acceleration (venturi) effect caused by the first two downstream turbines also plays an important role in wake recovery besides of the streamwise turbine spacing. Based on how one turbine wake interacts with its downstream turbine wakes, three different wake patterns are identified for staggered turbine arrays'.

For a given turbine occupied area, staggered turbine layout is preferred for locations without a fixed prevailing wind direction. An **aligned turbine array** with a **longer** streamwise turbine spacing, on the other hand, is suitable for locations with a **fixed prevailing wind direction. END**

From the above publication we have determined that for the East Wilmington field, with a prevailing wind there should be an aligned turbine array with as long a streamwise turbine spacing as possible, as shown below.

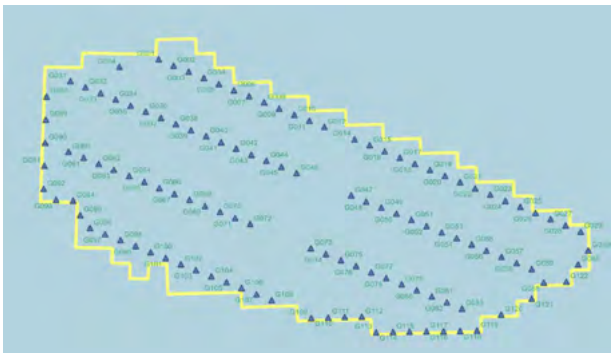

The layout as shown above has 122 Wind turbine generators (WTGs) laid out in 4 distinct rows. Each turbine is 1250M equidistant from its neighbour -side to side separation. The Gaps in the centre and front row are for 2 sub stations and export cables routing to shore, so as not to clash with the inter array cables.

The power Generation figures supplied for the East Wilmington Field are approximately 1.58 GW. Therefore, using the GE Haliade -X 13MW, would mean 1.3 GW or1300MW / 13MW = 122 WTG

APPENDIX VIII *Lighting*

See also **appendix x** Wind turbine external lighting regulations

There are two types of external lights on a wind turbine.

1. 2 aviation warning lights spec L864 fixtures; duty and standby mounted on the top of the Nacelle. They are of medium intensity flashing red.

2. 3 L810 marine traffic obstruction fixtures at 120-degree spacings around the perimeter of the tower, mounted midpoint between the sea and the underside of the nacelle. This number would increase to 4 should the diameter of the tower be more than 20 Feet.

The aviation lights will shine brightest in times of poor visibility, and their intensity will drop from 2000 candelas to 200 candelas in times of good visibility. This could drop further as our vertical field of view is less than 1% to the horizon.

Mitigation measures are shown in section 6.6 of **appendix xi**

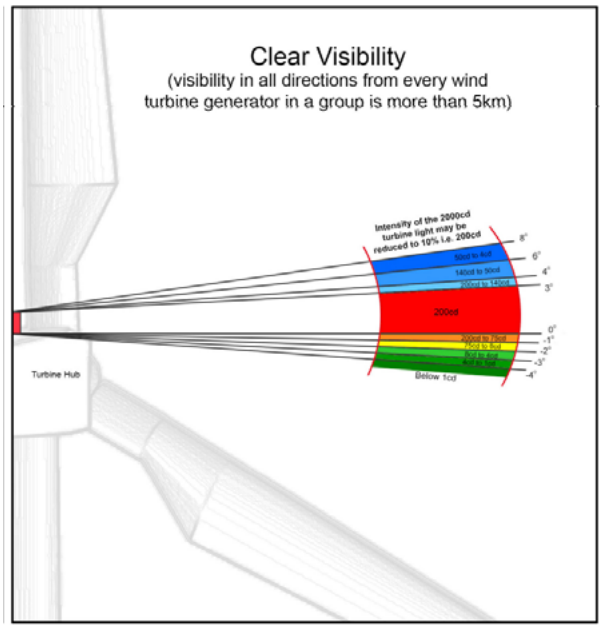

During times of clear visibility at night i.e., over 5KM, it is envisaged that any development designs and mitigates in the option to reduce the light Intensity by 90% down from 2000 to 200 Candelas or down to 2500 lumens, which is only 3 times more intense than a 60W light bulb.
Add to this the distance from the beach and vertical viewing angle of less than 1 Degree, this value could further reduce to 75 candelas .See above diagram.

(The lumen is the SI derived unit of luminous flux, a measure of the total quantity of visible light emitted by a source per unit of time.)

APPENDIX IX *Wind turbine external lighting regulations*

Wind Turbine External Lighting regulations

1) Lighting Standards. Aviation Obstruction Lighting.

Night-time offshore wind turbine obstruction lighting shall consist of **medium intensity** aviation red flashing, strobe, or pulsed LED obstruction lights meeting the minimum standards of the FAA L-864 fixture. Studies have shown that red lights provide the most conspicuity to pilots while also minimizing impacts to birds when flashed. To ensure compatibility with night vision goggles (NVG) the lights should incorporate LEDs that emit infrared energy between 675 and 900 nanometres.

Those commercial wind turbines expected to be installed beyond 12 NM are anticipated to be of a size and scale that will be significantly greater than 499 feet above mean sea level in overall height. As such, each wind turbine shall be lit to ensure that any obstructions are clearly marked and lighted in the airspace above 499 feet. In rare cases, not all wind turbine units within a wind turbine farm may need to be lighted. Such cases may include offshore wind farms which utilize smaller machines with overall heights of 499' or less, or which straddle the 12 NM jurisdictional boundary between FAA and BOEM, in which case the consistent lighting of the entire wind farm as one complete entity would take precedent. The decision to adopt one lighting standard or another would be determined on a case-by-case basis in consultation with FAA.

All aviation obstruction lighting should be automatically controlled utilizing GPS or other acceptable technology to be synchronized to flash simultaneously (within ±1/20 second (0.05 second) of each other). Controls shall include dry contact alarms for FLASH / FAIL monitoring and flash synchronization adjustability. The light intensity of all L-864 LED fixtures shall be automatically reduced (dimmed) based on meteorological visibility (i.e., clear sky conditions) to minimize visual impacts while maintaining adequate conspicuity to pilots. Visibility sensors and controls shall be installed which will allow light intensity to be lowered to 30% when visibility is more than 5 km (3.1 miles) and to 10% when visibility is more than 10 km (6.2 miles). In no instances shall the intensity be reduced to less than 200 candelas. The additional use of Aircraft Detection Lighting Systems (ADLS) to automatically activate the obstruction lights when approaching aircraft are detected until such time as they are no longer needed by the aircraft, is acceptable but not mandated. Any ADLS will need to conform with FAA guidance (see Chapter 14 of AC 70/7460-1L).

Should any lighting fixture or the lighting system synchronization fail, a lighting outage report should be prepared and submitted to the Bureau of Safety and Environmental Enforcement (BSEE).

Light fixtures should be placed as high as possible on the turbine nacelle, so they are visible to pilots from 360 degrees. (See Figure A-23 in Appendix A of AC 70/7460- 1L)

Daytime lighting of wind turbines is not required. See paragraph 13.4 for daytime marking requirements.

2) Wind Turbines Above 499 Feet. Redundancy.

For wind turbines with a rotor tip height, while at top dead centre, greater than 499 feet (153 m) Above Mean Sea Level (AMSL), but less than 699 feet AMSL, the turbines shall be lighted in accordance with paragraph 5.1. In addition to these requirements, the top of the turbine's nacelle shall be equipped with a second L-864 LED flashing red light. One of the two L-864 fixtures must be operating each night, with the second fixture serving as a backup in case the first experiences operational failure.

Duty and Standby. The two obstruction lights should be arranged horizontally, positioned on opposite sides of the nacelle, both be visible from 360 degrees, and have the same flash characteristic. (See Figure A-23 in Appendix A of AC 70/7460-1L) This lighting configuration ensures the turbines in this size category are always lighted.

In the event one of the two obstruction lights fails, no light failure notification is required; however, the light should be restored to service as soon as possible.

All turbines within this size category should be illuminated, regardless of their location within a wind turbine farm, and should be configured to flash simultaneously with the other turbines in the same farm. This requirement ensures the pilots operating at 500 feet AMSL have sufficient warning that a wind turbine obstruction may be within their flight path.

3) Wind Turbines at or Above 699 Feet (213 m). Low Intensity obstruction lighting

For wind turbines with a rotor tip height, while at top dead centre, at or above 699 feet (213 m) AMSL, additional lighting is required.

In addition to the lighting identified in paragraph 13.6, an additional level of lights is required at a point midway between the top of the nacelle and the water surface. The location of the additional lights may be adjusted as necessary to allow mounting at a seam within the turbine's mast.

The additional level of lights shall consist of a minimum of three (3) low intensity, aviation red flashing, strobe, or pulsed LED obstruction lights meeting the minimum standards of the FAA L-810 fixture, configured to flash in unison with each of the two L-864 red flashing lights located at the top of the nacelle. To ensure compatibility with night vision goggles (NVG) the lights should incorporate LEDs that emit infrared energy between 675 and 900 nanometres. The L-810s should be spaced at equal distances around the mast. The lights should be installed to ensure a pilot approaching from any direction has an unobstructed view of at least two of the lights. (See Figure A-23 in Appendix A of AC 70/7460-1L)

For wind turbine structures with a mast diameter greater than 20 feet (6 m), four L-810 red lights shall be used.

All turbines within this size category should be illuminated, regardless of their location within a turbine farm, and should be configured to flash simultaneously with the other turbines in the same farm. This requirement ensures the pilots operating at 500 feet AMSL have sufficient warning that a wind turbine obstruction may be within their flight path.

APPENDIX X *Lighting mitigation*

6.6.1 Mitigation Options

The options for mitigation of visual effects of aviation lighting that are currently available for the proposed Development are outlined in **Table TA6.2-2**. Mitigation measures that will be embedded in the project design are shaded in green. Mitigation measures that are being considered for the proposed Development, in discussion with regulators, are shown in grey.

Table TA6.2-2 Turbine Lighting Mitigation Options

Mitigation Option	How it works
Reduce intensity of lights from 2,000cd to 200cd	Already provided for in CAA guidance CAP 393. 2,000cd aviation lights may be dimmed to 10% of their intensity (200cd) in where visibility conditions permit, when visibility from every turbine within the wind farm group is >5km. Visibility conditions are measured using a visibility sensor, which can then be dimmed automatically to respond to prevailing meteorological conditions. 2,000cd lights will therefore only be experienced in visibility of <5km; and their intensity would be dimmed to 200cd in visibility of >5km.
Directional intensity	Established in ICAO (Annex 14) guidance. This focusses the 2,000 cd lighting in the horizontal plane (+ or – a few degrees) and reduces the intensity of the light from above and from below the horizontal plane. Most current aviation light models on the market will incorporate this as standard, for example, LuxSolar Medium Intensity Obstruction Light and Obelux Medium-Intensity Red Obstruction Light.
'Smart' aviation lighting (or 'surveillance activated') (aviation obstruction lighting detection system)	'Smart' aviation lighting would only be switched on when aircraft approach a defined airspace around the wind farm. The CAA is in the process of consulting on a new policy statement on En-Route Aviation Detection Systems for Wind Turbine Obstruction Lighting Operation. The draft guidance would allow the aviation lights only to be illuminated when an aircraft is detected by a surveillance system entering a volume bounded by 4 km (horizontal distance) from the perimeter turbines and 300m above the highest turbine tip of the Site. The aviation lighting would not be activated when commercial airlines pass over the Site as such aircraft ordinarily operate in Controlled Airspace (CAS).